



Single-cell transcriptomic identified HIF1A as a target for attenuating acute rejection after heart transplantation

Yuan Chang^{1,3} · Xiangjie Li^{2,3} · Qi Cheng^{4,5} · Yiqing Hu³ · Xiao Chen³ · Xiumeng Hua³ · Xuexin Fan³ · Menghao Tao³ · Jiangping Song³ · Shengshou Hu^{1,3}

Received: 11 May 2021 / Revised: 4 November 2021 / Accepted: 20 November 2021 / Published online: 6 December 2021
© The Author(s), under exclusive licence to Springer-Verlag GmbH Germany 2021

Abstract

Acute rejection (AR) is an important contributor to graft failure, which remains a leading cause of death after heart transplantation (HTX). The regulation of immune metabolism has become a new hotspot in the development of immunosuppressive drugs. In this study, Increased glucose metabolism of cardiac macrophages was found in patients with AR. To find new therapeutic targets of immune metabolism regulation for AR, CD45⁺ immune cells extracted from murine isografts, allografts, and untransplanted donor hearts were explored by single-cell RNA sequencing. Total 20 immune cell subtypes were identified among 46,040 cells. The function of immune cells in AR were illustrated simultaneously. Cardiac resident macrophages were substantially replaced by monocytes and proinflammatory macrophages during AR. Monocytes/macrophages in AR allograft were more active in antigen presentation and inflammatory recruitment ability, and glycolysis. Based on transcription factor regulation analysis, we found that the increase of glycolysis in monocytes/macrophages was mainly regulated by HIF1A. Inhibition of HIF1A could alleviate inflammatory cells infiltration in AR. To find out the effect of HIF1A on AR, CD45⁺ immune cells extracted from allografts after HIF1A inhibitor treatment were explored by single-cell RNA sequencing. HIF1A inhibitor could reduce the antigen presenting ability and pro-inflammatory ability of macrophages, and reduce the infiltration of *Cd4+* and *Cd8a+* T cells in AR. The expression of *Hif1a* in AR monocytes/macrophages was regulated by pyruvate kinase 2. Higher expression of HIF1A in macrophages was also detected in human hearts with AR. These indicated HIF1A may serve as a potential target for attenuating AR.

Keywords Heart transplantation · Acute rejection · HIF1A · Immune metabolism

✉ Jiangping Song
fwsongjiangping@126.com

- ¹ Union Hospital, Tongji Medical College, Huazhong University of Science and Technology, Wuhan 430000, China
- ² School of Statistics and Data Science, Nankai University, Tianjin 300371, China
- ³ The Cardiomyopathy Research Group at Fuwai Hospital, State Key Laboratory of Cardiovascular Disease, National Center for Cardiovascular Diseases, Chinese Academy of Medical Sciences and Peking Union Medical College, Beijing 100000, China
- ⁴ Hepatic Surgery Center, Tongji Hospital, Tongji Medical College, Huazhong University of Science and Technology, Wuhan 430000, China
- ⁵ Key Laboratory of Organ Transplantation, Ministry of Education, Chinese Academy of Medical Sciences, Ministry of Education, National Health Commission, Wuhan 430000, China

Introduction

Heart transplantation (HTX) remains the ultimate treatment option for patients with advanced heart failure, which is defined as the presence of progressive and/or persistent severe signs and symptoms of heart failure despite optimized medical, surgical, and device therapy [9, 46]. In patients who undergo HTX, acute rejection (AR) accounts for about 11% of deaths in the first 3 years. Moreover, recurrent AR has a cumulative immune injury effect on the onset of cardiac allograft vasculopathy, which is an important contributor to graft failure [24, 35, 44].

AR is a T cells-mediated adaptive immune response, donor derived antigens are presented to the recipient's T cells by donor and recipient antigen-presenting cells, which leads to activation of T cells [43]. Current immunosuppressants are primarily targeted against the adaptive immune system [51], but a growing body of evidence shows that the

innate immune response contributes to graft injury in AR [32]. Damage-associated molecular patterns (DAMPs) are released following ischemia/reperfusion injury (IRI) during the HTX procedure. DAMPs are recognized through pattern recognition receptors (PRRs) on the cell surface and in the cytoplasm of innate immune cells. This process will activate the innate immune cells, assisting the occurrence of AR [42]. It is important to note that the innate immune response in AR cannot be fully explained by IRI. Deletion of MyD88 which is an important PRR adaptor did not attenuate rejection [27]. The latest research also found that monocytes and macrophages could acquire memory specific to major histocompatibility complex I (MHC-I) antigens, which was called innate myeloid cell memory. Blocking this recognition attenuates kidney and heart allograft rejection [11]. Other innate immune cells, such as natural killer (NK) cells, are also been found in the allograft heart, which can promote expansion and effector function of alloreactive T cells [28]. Therefore, immunosuppressants targeting the innate immune system are worth developing.

Current immunosuppressants mainly target the antigen presentation process and its cascade signaling pathways, such as calcineurin-NFAT pathway, mTOR pathway, and DNA synthesis process. The new concept of immunometabolic research is gaining interests. Activated immune cells need to remodel their metabolic state because their energetic and synthetic demands are higher than those of resting cells. This offers the opportunity for preventing and treating inflammatory diseases by manipulating the metabolic process of immune cells [31]. This approach may have great promise for improving the prognosis for transplant patients, but the theories of immunometabolic regulation have not been explored in transplant immunology.

The immune cell populations, transcriptome, and metabolic activity in allografts are complicated, and their roles in hearts with AR are difficult to interpret by the traditional approach. Single-cell RNA sequencing (scRNA-seq) has been developed, in which a large number of gene expressions in thousands of individual cells can be measured simultaneously [26]. This approach offers an opportunity to define cell types and states comprehensively in hearts with AR.

In human heart samples with AR, we observed high abundance of pyruvate kinase (PKM) in macrophages by immunostaining. This indicated glucose metabolism was increased in graft-infiltrating macrophages, despite treated by immunosuppressive therapy. To further explore the mechanism of AR, scRNA-seq of immune cells was performed from isografts, allografts, and untransplanted donor hearts. We revealed the whole landscape of immune cells during the AR at a single-cell resolution. A significant increase of glycolysis level in monocytes/macrophages was observed in allografts. *Hif1 α* was found to be highly expressed gene in monocytes/macrophages in allografts and regulate the

expression of glycolysis-related genes. HIF1A inhibitor could alleviate inflammatory levels of AR. By scRNA-seq of immune cells in allografts treated with HIF1A inhibitor, we found that inhibition of HIF1A could attenuate antigen presentation and pro-inflammatory effects of macrophages. We next confirmed that the expression of *Hif1 α* was regulated by PKM2, a key rate-limiting enzyme of glycolysis. *Hif1 α* and glycolysis formed a positive cycle to regulate energy metabolism of monocytes/macrophages. HIF1A was expressed at higher levels in human hearts with AR than that in healthy hearts. Taken together, HIF1A-dependent activation of macrophages may play a catalytic role in AR, which may serve as a promising therapeutic target for preventing AR.

Methods

Human heart sample collection

The use of human tissue in the present study was approved by the Human Ethics Committee of Fuwai Hospital, Chinese Academy of Medical Sciences. Written informed consent was obtained from each patient. Human AR heart samples ($n=3$) were collected from patients who had undergone secondary HTX due to AR. Healthy heart samples ($n=4$) were obtained from brain-dead donors with a normal circulatory supply who were not suitable for transplantation due to technical or noncardiac reasons.

Mice

Male C57BL/6J and BALB/c mice with a bodyweight of 25–28 g at 10–12 weeks of age were used for this study. Animals were purchased from the Charles River Laboratories (Beijing, China). All animals were cared for in a specific pathogen-free facility and were approved by the Animal Ethics Committee at Fuwai Hospital.

HTX in mice

All animals were anesthetized with an intraperitoneal injection of pentobarbital and placed supine on the operative field. The donor surgery was done as follows: a midline abdominal incision was made, 1 ml of ice-cold heparin (10 U/ml) was injected through the inferior vena cava. Next, the thoracotomy was performed. The heart was perfused with 4 °C saline solution to remove the blood. The inferior vena cava, the superior vena cava, the pulmonary veins, and the azygous vein are ligated with 6-0 silk and divided superior to the ligatures. The donor's heart was harvested after dissection of the ascending aorta and pulmonary artery. Store the heart in ice-cold solution. For the recipient, along midline abdominal incision was made. Abdominal viscera were put

outside the abdomen with gauze to expose the abdominal aorta and the inferior vena cava. The ascending aorta and the pulmonary artery of the donor's heart were anastomosed end to side to the abdominal aorta and the inferior vena cava, respectively. Allogenic HTX was performed to induce severe AR (donor BALB/c; recipient C57BL/6J). Isogenic HTX was performed to rule out IRI (donor BALB/c; recipient BALB/c).

Tissue processing and single-cell dissociation

7 days after HTX, surgically excised the explanted hearts. The hearts were rinsed to remove the blood by ice-cold phosphate buffer, then collected in DMEM media (11885084, Gibco) containing 10% fetal bovine serum (35-076-CV, Corning). Remove the great vessels and atrial tissue, then an approximately 1-mm-thick cross-section of the myocardium was cut from the middle of the heart and fixed with 4% paraformaldehyde overnight. Tissues were processed into paraffin sections for pathological staining. The remaining sections of hearts tissues were prepared for single-cell suspensions.

We pooled five hearts together from each group, the heart tissues were minced into small pieces and incubated at 37 °C in 10 ml freshly prepared enzyme buffer containing 200 U/ml collagenase type II (LS004176, Worthington). Cells in the supernatant were harvested every 15 min by filtering the cells through a 40 µm cell strainer (352340, Falcon) into equal volume of 10% FBS/DMEM. The residual tissues on the cell strainer were dissociated again for 15 min, then filtered the cells into the 10% FBS/DMEM. Repeat this procedure three times until most of tissue had been dissociated into single cells. Finally, cells were collected by centrifugation at 300×g for 5 min, the pellets were resuspended in 1 ml of 10% FBS/DMEM.

Flow cytometry and fluorescence-activated cell sorting

For scRNA-seq, non-cardiomyocyte suspension was stained by dyeing buffer containing anti-CD45-FITC (564590, BD Biosciences) at a dilution of 1:200 per 10⁶ cells, and incubated on ice for 20 min in dark, then washed cells by PBS twice. Resuspended the pellets in 600 µl PBS containing 30 µl 7-AAD (559925, BD Biosciences) before FACS. The stained cells were analyzed and sorted by FACS Aria II cell sorter (BD Biosciences). The CD45⁺ and 7-AAD⁻ immune cells were sorted for scRNA-seq. Finally, cell viability was more than 90% assessed by Trypan Blue staining before scRNA-seq. For identification of the inflammatory cells proportion, non-cardiomyocyte suspension were stained by anti-CD45-FITC antibody (564590, BD Biosciences) at a dilution of 1:200 per 10⁶ cells, the proportion of inflammatory cells was the proportion of CD45⁺ cells to total

non-cardiomyocytes. For fate-mapping macrophages, non-cardiomyocyte suspension was stained by anti-CD11b-PE (120112-82, ThermoFisher) and anti-LY6C-APC (175931-82, ThermoFisher). Fate-mapping macrophages which came from recipients were FITC beads positive. For sorting LY6C⁺ macrophages in allografts, non-cardiomyocyte suspension was stained by anti-CD45-FITC antibody (564590, BD Biosciences), anti-CD11b-PE (12-0112-82, ThermoFisher), and anti-LY6C-APC (17-5931-82, ThermoFisher). CD45⁺, CD11b⁺ and LY6C⁺ macrophages were sorted.

Histology and morphology

For each control heart or graft, an approximately 1 mm-long cross-sectional tissue were taken, and fixed into formalin for 24 h, then embedded in paraffin, then serially sectioned at 4-µm thickness. Serial sections were stained with hematoxylin and eosin (H&E) to determine the inflammatory phenotype and structure. The established inflammatory score (0: no inflammatory infiltrates; (1) 1–5 distinct mononuclear inflammatory area, with the involvement of 5% or less of the cross-sectional area of the heart; (2) more than five distinct mononuclear inflammatory areas, or the involvement of over 5% but not over 20% of the cross-sectional area of the heart; (3) profound mononuclear infiltration involving over 20% of the area, without necrosis; (4) diffuse inflammation with necrosis in the heart) was used to evaluate leukocyte infiltration semi-quantitatively as previously described [6].

Immunohistochemistry stain

About 3-µm-thick sections were prepared and collected on poly-lysine-coated slides. Antigen repair was performed using EDTA solution (pH 9.0, ZLI-9068, ZSBG-BIO, China). The endogenous peroxidase activity was blocked by 3% hydrogen peroxide for 20 min, and nonspecific binding was blocked by the use of goat serum (ZLI-9056, ZSBG-BIO, China) for 45 min. Sections were stained with anti-rabbit CD3 (ab31630, Abcam, UK), anti-mouse HIF1A (ab1, Abcam, UK), followed by anti-rabbit-HRP (PV-6001, ZSBG-BIO, China) or anti-mouse-HRP (PV-6002, ZSBG-BIO, China) and chromogenic DAB staining, respectively. Immuno-positive cells and areas were quantified using Image-pro plus software.

Multiplex immunofluorescence staining

The Opal 7 multiplexed assay (PerkinElmer, MA, USA) was used to generate multiple staining slides. The best concentration of antibodies was determined before multiplex staining, including CD3 (ab16669, Abcam, 1/100), CD68 (ab31630, Abcam, 1/100), HIF1A (Abcam, ab1, 1/50), PKM (Abcam,

ab150377, 1/400), CCR2 (Abcam, ab273050, 1/400). Nuclei were stained with DAPI. The detection for each marker was completed after the application of all antibodies. The slides were scanned at high resolution using Vectra3 with a 20× or 40× objective.

LW6 treatment

The compound LW6 was purchased from MedChem Express (HY-13671, MCE). Allogenic HTX was performed, and the mice were randomly assigned to two groups, the LW6 treat group and the no treat group. LW6 was dissolved into vehicle solution containing 10% dimethylacetamide, 5% Tween-80, and 85% of saline. Intraperitoneal injection: no treat group, vehicle solution; LW6 treat group, LW6 at a dose of 20 mg/kg once a day. The treatments were continued for 7 days after HTX surgery.

TEPP46 treatment

The compound TEPP46 was purchased from MedChem Express (HY-18657). Allogenic HTX was performed, and the mice were randomly assigned to two groups, the TEPP46 treat group and the no treat group. TEPP46 was dissolved into vehicle solution containing 7% dimethylsulfoxide, 5% Tween-80, and 20% PEG300, and 68% of saline. Intraperitoneal injection: no treat group, vehicle solution; TEPP46 treat group, TEPP46 at a dose of 100 mg/kg once a day. The treatments were continued for 7 days after HTX surgery.

Single-cell RNA sequencing

Single-cell suspensions were loaded on the Chromium Single Cell Controller (10× Genomics) to generate a single cell and gel bead emulsion (GEM). scRNA-seq libraries were prepared using the Single Cell 5' PE (V3.0.2). GEM reverse transcription was performed by the thermal cycler (Bio-Rad C1000 Touch) running the following program: 53 °C for 45 min and 85 °C for 5 min, held at 4 °C. Following reverse transcription, GEMs were broken, and single-strand cDNA was purified with DynaBeads Myone Silane Beads. cDNA was amplified with the thermal cycler: 98 °C for 3 min, 14 cycles of 98 °C for 15 s, 67 °C for 20 s, 72 °C for 60 s; 72 °C for 1 min, and held at 4 °C. Subsequently, cDNA was cleaned up using the SPRIselect reagent kit (Beckman Coulter), quantified, and quality controlled with the Agilent Bioanalyzer High Sensitivity Kit. Indexed sequencing libraries were prepared by Single Cell 5' PE (V3.0.2): (1) enzymatic fragmentation, (2) end repair, (3) A-tailing, (4) adaptor ligation, (5) post ligation cleanup—SPRIselect. (6) sample index PCR, (7) post sample index PCR cleanup—SPRIselect, (8) post library construction QC. 5' Gene Expression libraries comprise standard Illumina paired-end constructs which

begin with P5 and end with P7. 16 bp 10× Barcodes are encoded at the start of Read 1, while sample index sequences are incorporated as the i7 index read. Read 1 and Read 2 are standard Illumina sequencing primer sites used in paired-end sequencing. Read 1 is used to sequence 16 bp 10× Barcodes and 10 bp UMI.

scRNA-seq data preprocessing

10× sequencing data were performed using Cell Ranger Single-Cell Software (version 3.0.2, 10× genomics) with mm10 mouse reference genome for each sample group. We used the default parameters for cellranger. Cells with fewer than lower UMI counts were filtered automatically by *cellranger*. We further filtered out cells with the number of expressed genes < 800 or the number of UMI < 1000 or the percentage of mitochondrial > 10% or the number of expressed genes > 5000 or the number of UMI > 50,000. Doublets were detected with Scrublet approach [52].

Dimension reduction and clustering of scRNA-seq data

Based on the above preprocessing, we conduct clustering for the remaining cells. Gene expression values (or UMI count matrix) for each cell were normalized to count-per-ten-thousand, log-transformed by *NormalizeData* function in Seurat v3.0.2. A set of highly variable genes was identified by *FindVariableFeatures* with parameter *nfeatures* = 3000. Using these highly variable genes, we integrated data *FindIntegrationAnchors* and *IntegrateData* functions in Seurat with 50 dimensions to use from the CCA to specify the neighbor search space [47]. The integrated data were scaled, and principal component analysis was run on the scaled data for the set of previously defined highly variable genes. To identify the number of principal components (PCs) to use for clustering, we ran the *JackStraw* and *ScoreJackStraw* procedure implemented in Seurat, combined with variance contribution ration that identified 55 statistically significant PCs. The selected 55 PCs were feed in *FindNeighbors* with *k.param* = 25, *RunUMAP* with *n.neighbors* = 25, *FindClusters* with *resolution* = 0.1 to 1.0 step by 0.1. Finally, we used *resolution* = 0.5 as the final clustering results. For clustering, we also experimented with modifying the number of PCs (40, 50 and 60) but found that varying the number of PCs caused only minor impact on the clustering results. UMAP visualization was used for show cells' labels and groups. Cell identity was assigned by manual annotation using known marker genes and computed DEGs (differential expression genes). The DEGs for each cluster were computed in at least 10% of cells in either of the two populations compared and the expression fold change at least exp(0.6).

Supervised clustering method

Before and after annotation, a cluster or cell type classifier was built by training two supervised learning tools, RandomForest and xgboost, to look the accuracy and stability of clustering and cell type annotation. As commonly setting in supervised learning, we split the training data and testing data (the selected 55 PCs) into 70% and 30%, respectively. We take cluster id as the true label for clustering results, and we show that the accuracy of testing data of both RandomForest and xgboost can reach 90% on primary clustering results. As for cell type annotation, the accuracy of RandomForest and xgboost can achieve to 0.93.

Gene scores

Enrichment scores were calculated using Seurat function 'AddModuleScore'. 'AddModuleScore' function calculated the average expression of a gene set subtracting the aggregated expression of control gene sets, which could be deemed as the average relative expression. Gene lists were in Online-only Table I.

Differential expression analysis

Differential expression (DE) tests for a gene between a pair of clusters or between a cluster and the remaining clusters were performed using the *FindAllMarker* function in Seurat package (with default test method Wilcoxon rank sum test, p values were adjusted for multiple testing using the Bonferroni correction).

Differential proportion analysis

We adopted an approach for detecting changes in populations across different conditions [12]. Cells were assigned two labels: a group (G) label representing experiment group/condition and a cell type label (L). A count table was generated for each cluster per condition, and then computed the proportion of cell types in different conditions, respectively. We defined statistics for the differential proportion test, $\Delta_{p_j} = p_j^{C_1} - p_j^{C_2}$ as the difference in cluster proportions between two conditions C_1 and C_2 , where $p_j^{C_1}$ and $p_j^{C_2}$ are corresponding proportions in condition C_1 and condition C_2 for some cluster j . Then Farbehi et al. [12] construct a null distribution for Δ_{p_j} by randomly permuting cluster labels L for some w proportion of n total cells. Specifically, we randomly selected $w \times n$ cells and replaced their cell-type labels by the labels randomly chosen from all the cells (sampling without replacement). A new count and proportion table was then generated from this randomized sample. Here we used

$w=0.3, 0.24, 0.2, 0.15, 0.1, 0.05$ and repeat 50,000 times for each value, and then the resulting Δ_{p_j} across the randomized data forms the null distribution.

After constructing null distribution, we then calculated empirical p values representing either an increase or decrease in Δ_{p_j} such that $p_{\text{increase}} = \frac{1}{50,000} \sum_{b=1}^{50,000} I(\Delta_{p_b} \geq \Delta_{p_j})$, $p_{\text{decrease}} = \frac{1}{50,000} \sum_{b=1}^{50,000} I(\Delta_{p_b} \leq \Delta_{p_j})$, where $I(\bullet)$ was the indicator function. A final p value, p_j can be defined as the minimum of p_{increase} and p_{decrease} .

SCENIC analysis

We applied single-cell regulatory network inference and clustering (SCENIC) analysis to identify which transcription factors (TFs) for some major cell types (Macrophage, Neutrophils, T cells, NK cells, DC cells) [1]. For each major cell type, we conducted SCENIC analysis for three groups, respectively. When focusing on TFs interaction, we only considered those TFs with $\text{TF_score} > 0.5$ and target genes with $\text{Target_score} > 0.5$. The database, including motif, TSS+10 kb, TSS +/5 kb, and mouse TFs can be downloaded from <https://www.resources.aertslab.org/cistarget/>.

RNA velocity analysis

We conducted RNA velocity analysis for Macrophage. Specifically, the bam files produced by a standard pipeline of *cellranger* for each group can be fed into *velocity* (version 0.17.17) using *run10x* command to obtain spliced and unspliced information. And then we used the standard pipeline of *scvelo* (version 0.1.24) to obtain the latent time of the macrophage cell type (combined M1–M9). Note that we used the *scvelo.pp.filter_normalize* function with parameters *min_shared_counts*=20 and *n_top_genes*=2000 and *scvelo.pp.moments* function with *n_pcs*=30 and *n_neighbors*=30. We used the default values for other functions in *velocity*.

Cell–cell interaction analysis

Cell–cell interaction weights were computed by the product of the fold change of ligands in sender-cell types and the fold change of the corresponding receptors in receiver-cell types. And the ligand receptor database was download from CellPhoneDB.

Gene ontology analysis

Over-representation of GO terms in gene lists was calculated using the *enrich* Go function in R package clusterProfiler. Gene symbol was firstly converted into entrezid by

bitr function in clusterProfile. We only show top few significant go term (sort *p* value in increasing order, and limit *p* value < 0.05) unless otherwise stated.

RNA isolation and real-time quantitative PCR

Total RNA was extracted using RNeasy Mini Kit (74104, Qiagen) following the manufacturer's protocol. RNA was reverse transcribed using PrimeScript™ RT Master Mix (RR036A, Takara). For real-time quantitative PCR, cDNA was amplified by powrup SYBR master mix (A25742, ThermoFisher) and run on Applied Biosystems QuantStudio 5 thermocycler. Rps18 gene were used as reference gene. Relative quantitation values were calculated using the $2^{-\Delta\Delta Ct}$ method.

Bone marrow-derived macrophages (BMDM) culture and polarization

Bone marrow cells were collected from femur and tibia bones from 6 to 8 weeks old C57BL/6J mice. BMDM were induced polarization in Dulbecco's modified eagle medium (DMDM) + 10% FBS + 1% penicillin and streptomycin solution + 100 ng/μl monocyte-colony stimulating factor (M-CSF, 51112-MNAH, SinoBiological) for 7 days.

IFN-γ and cardiac antigen induced activation of BMDM

0.2 g fresh heart fragments of BALB/c were cut with ophthalmic scissors in 600 μl PBS and homogenized using MagNA Lyser (Roche). The homogenate was centrifugated at 3000 rpm for 4 min and the supernatant liquid was filtered by 0.22 μm filter (SLGV033NS, Merck). The filtered supernatant was used as cardiac antigen. Polarized BMDM was acquired as above. The activation of BMDM was cultured in DMEM + 10%FBS + 1% Penicillin&Streptomycin solution + 20 ng/μl M-CSF + 20 ng/μl IFN-γ + 2.5% cardiac antigen solution for 48 h. The concentration of LW6 treatment was 10 μmol/L.

Cardiomyocytes and BMDM co-culture

Cardiomyocytes were isolation from Balb/c mice using neonatal heart dissociation kit following the manufacturer's protocol (130-098-373, Miltenyi). Six-well plate seeded with 1 million cardiomyocytes per well in DMEM + 10%FBS + 1% Penicillin&Streptomycin solution. 1 day later, 0.5 million polarized BMDM per well were added to the cardiomyocytes culture medium. LW6 (10 μmol/l) was added at same

time. The death of cardiomyocytes was identified by flow cytometry with 7AAD staining.

Fate-mapping of monocytes

C57BL/6J mice were injected intravenously with 200 μl of 0.5 mm-microsphere fluoresbrite YG beads (18859-1, Polysciences; diluted 1:10). Injected beads could be captured by blood monocytes. 1 h later, C57BL/6J mice injected with beads was used as recipients for HTX experiments to receive Blab/c mouse heart. Mice were sacrificed 7 days after HTX, allografts harvested, and the frequency of fluorescent beads macrophages in allografts determined by flow cytometry.

Survival analysis

LW6 was administered daily in allogenic HTX, and vehicle solution was administered daily in allogenic HTX as control. Grafts were touched daily until it stopped beating, and the survival time of the graft was recorded.

Statistical analysis

For non scRNA-seq data analysis, two-group comparisons, an unpaired, two-tailed Student's *t* test was used. Multiple group comparisons were made by one-way ANOVA. Survival analysis was performed by Kaplan–Meier. All values are presented as the mean ± SEM; *n* refers to the sample size. A value of *p* < 0.05 was considered statistically significant. For scRNA-seq data analysis, all statistical analysis was performed in R. Statistical significance was accepted for *p* < 0.05.

Results

Glucose metabolism of macrophages elevated in patients with AR

Explanted hearts were collected from patients receiving a second heart HTX due to AR. All patients had defined pathological features of AR, such as focal inflammatory cell infiltration and cardiomyocyte destruction, despite receiving immunosuppressive therapy (Fig. 1a). Besides T cells (CD3⁺), a large number of macrophages (CD68⁺) infiltrated in the explanted hearts with AR (Fig. 1b, c). PKM was highly expressed in AR, especially in macrophages (Fig. 1d). These results suggested that the glucose utilization of graft-infiltrating macrophages is higher in AR.

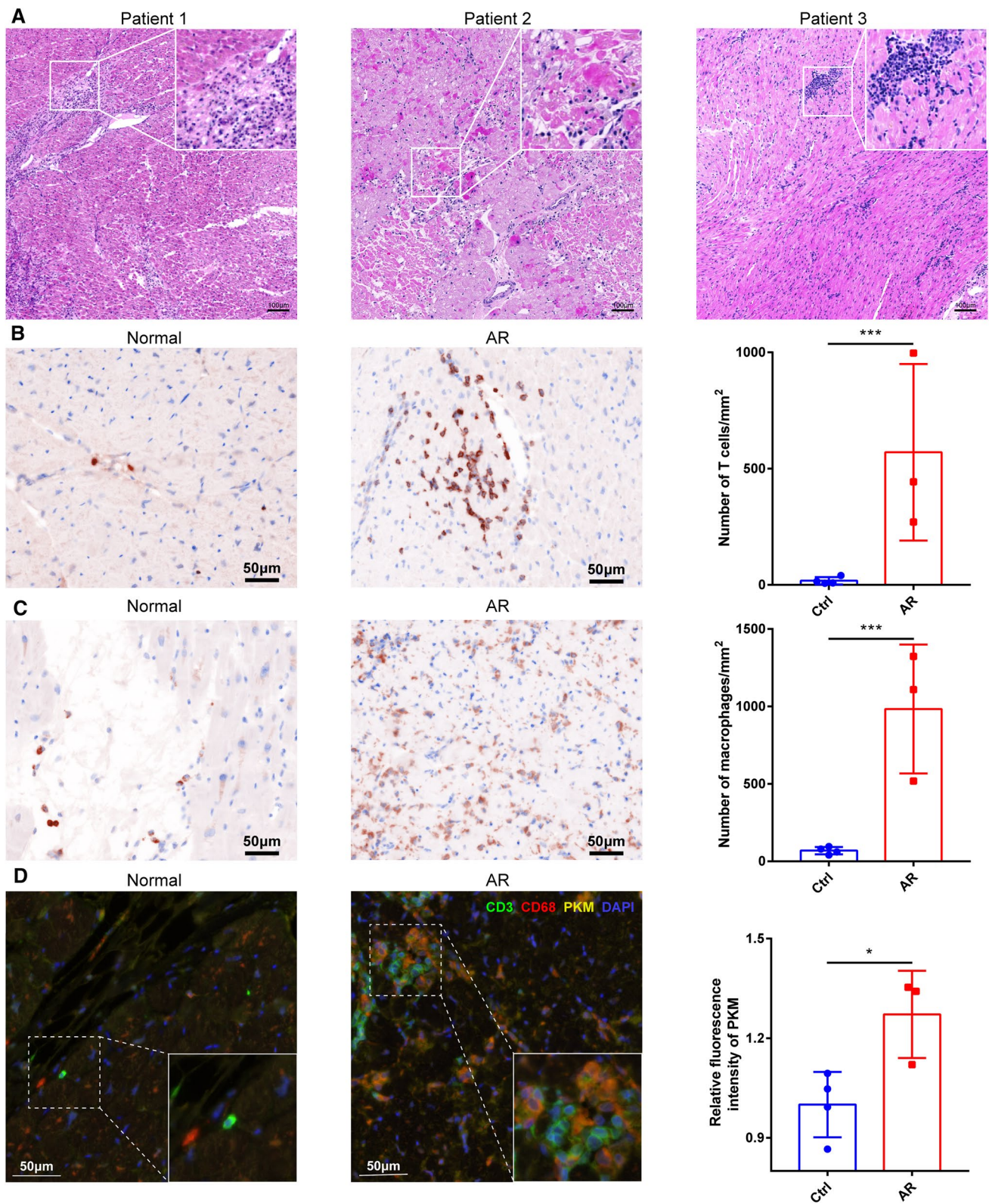


Fig. 1 Pathological staining for hearts from AR patients and normal people. **a** HE stain for heart tissue from patients with AR, **b** CD3 staining for hearts from normal people ($n=4$) and AR patients ($n=3$). **c** CD68 staining for hearts from normal people ($n=4$) and

AR patients ($n=3$). **d** The expression of PKM in T cells (CD3 positive) and macrophages (CD68 positive) in hearts from normal people ($n=4$) and AR patients ($n=3$) (* $p<0.05$, ** $p<0.01$, *** $p<0.001$)

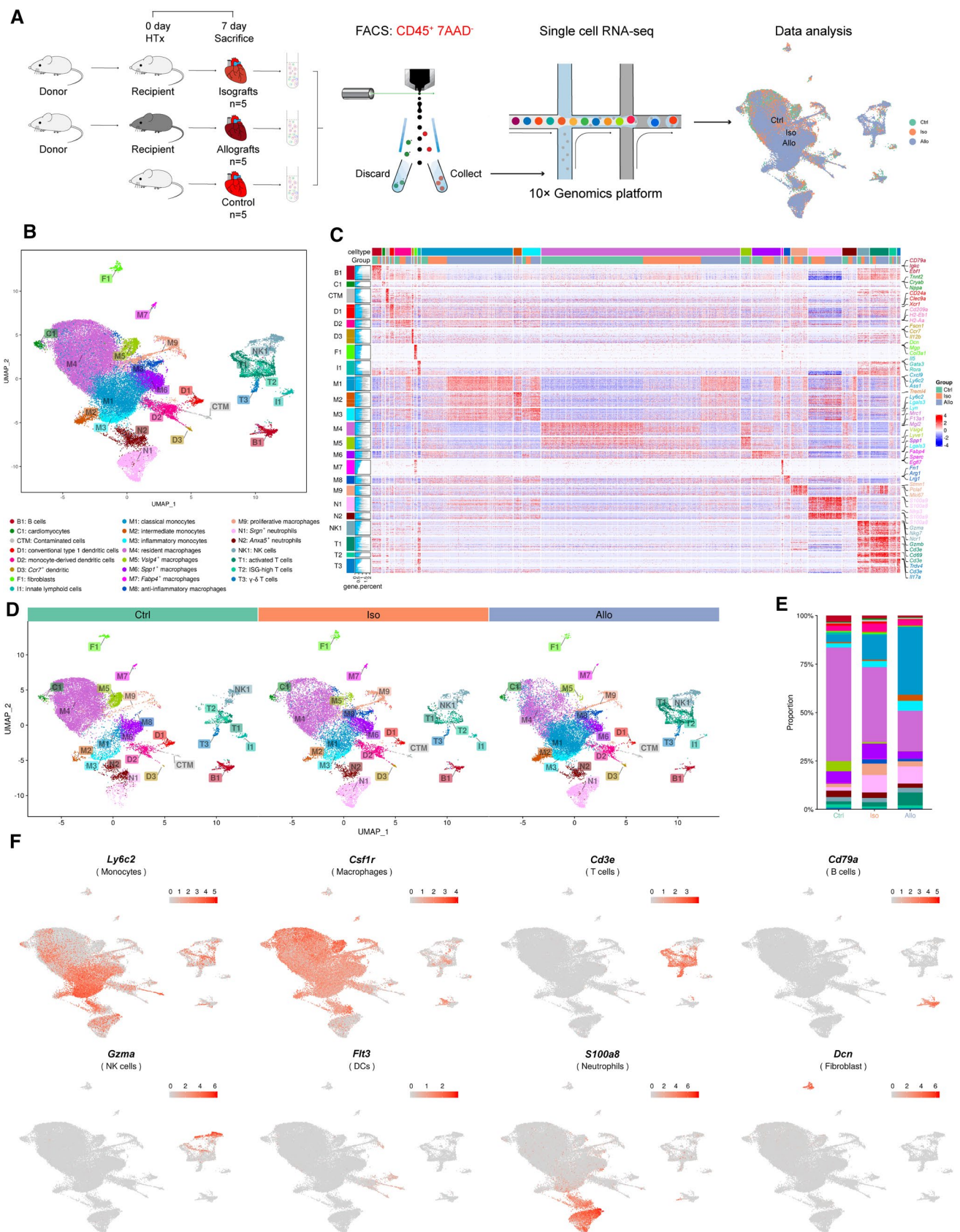


Fig. 2 Overview of the 46,040 single cells isolated from mice HTX model. **a** Study design of scRNA-seq in mice HTX model. **b** UMAP plot of the 46,060 immune cells, colors coded for cell type. **c** Gene-expression heatmap of the marker genes for 23 cell types. **d** UMAP plot for each experimental group, Ctrl, normal hearts; Iso, Isografts, Allo, allografts. **e** The percentage change tendency of each cell type among three groups. **f** Expression of classical marker genes used to define cell type. *FACS* flow cytometry and fluorescence activated cell sorting, *DCs* dendritic cells, *ILCs* innate lymphoid cells, *NK* natural killer

Total cardiac immune cell populations in hearts with AR

For searching potential therapeutic targets, we constructed mice models of HTX. According to the histological analysis, AR only happened in allografts, with obvious inflammatory cell infiltration and myocardial cell necrosis (Suppl. Figure 1A–D). Considering the sex mismatch in clinical situation, we also constructed sexually mismatched allografts, including male donor heart to female recipient and female donor heart to male recipient. These two situations showed no differences in inflammatory cell infiltration (Suppl. Figure 1E–G). Previous studies have shown that the survival time of allografts was associated with recipient estrogen level over chromosomal sex mismatches [25, 60]. Estrogen levels are influenced by the menstrual cycle and age. To exclude estrogenic interference, we finally chose male to male HTX model for further studies. ScRNA-seq was performed on the cardiac immune cell population (CD45⁺) from allografts, isografts, and untransplanted hearts (Fig. 2a). Transcriptional profiles of 46,040 cells (allografts: 16,972; isografts: 13,480; control: 15,588) were captured after quality control. 23 cell clusters were identified according to the well-characterized marker genes and the enrichment function of each cell type (Fig. 2b, c). No significant intergroup batch effect was observed (Fig. 2d). The most abundant cell populations were monocytes/macrophages (M, nine clusters), followed by neutrophils (N, two clusters), T cells (three clusters), dendritic cells (DCs, three clusters), B cells (one cluster), natural killer (NK) cells (one cluster), innate lymphoid cells (ILCs, one cluster), cardiomyocytes (one cluster), fibroblasts (one cluster), and contaminated cells (one cluster) (Fig. 2e, f). A cluster of contaminated cells was excluded from the downstream analysis with the expression of multiple lineage markers, such as *Cd8b1*, *Igk3*, and *Cd209d*.

The phenotypic shift of monocytes/macrophages in AR

We defined nine transcriptional states of monocytes/macrophages (Fig. 3a). The gene expression pattern was different among monocytes/macrophages subclusters. M1 expressed

high levels of *Ly6c2* and *Ccr2*, which indicated these clusters belonged to classical monocytes (Fig. 3b, d). M2 expressed *Ly6c2* and *Trem14*, which was defined as intermediate monocytes [19] (Fig. 3b, d). M3 also expressed *Ly6c2* and *Ccr2* but had completely different functions compared to M1, M3 is mainly associated with inflammatory response, including response to interferon, leukocyte chemotaxis, and regulation of innate immune response (Suppl. Figure 2A). M4 highly expressed markers of resident macrophages, including *ApoE*, *F13a1*, *Mgl2*, *Cd163*, and *Pf4*, and with the low expression of *Ly6c2* and *Ccr2* (Fig. 3b, d). M5 expressed *Vsig4* (Fig. 3b), which was reported to inhibit pro-inflammatory macrophage activation [14, 20]. M6 expressed *Spp1* and *Lgals3* (Fig. 3b), which was implicated in the phagocytic clearance of dead cells and reparative fibrosis [41]. M7 expressed *Fabp4*, *Gpihbp1*, *Sparc*, and *Egfl7* (Fig. 3b). M8 expressed the marker genes associated with anti-inflammation, including *Fnl*, *Arg1*, *Lrg1*, and *Olr1* (Fig. 3b). We calculated the pathway enrichment scores of cell-cycle in monocytes/macrophages, M9 represented the dividing cell, which had the highest cell-cycle score (Fig. 3e).

The proportion of *Ly6c2*⁺ and *Ccr2*⁺ cells (M1, M2, and M3) all increased in allografts compared with that in isografts (Fig. 3c). CCR2⁺ and CD68⁺ monocytes/macrophages were confirmed by immunofluorescence to be increased in allografts (Suppl. Figure 3A–C). To find out the origin of these cells, we performed fate mapping of monocytes in recipients. Blood monocytes of recipients were specifically labeled by the intravenous injection of fluorescent latex beads 1 h before HTX (Suppl. Figure 3D). Flow cytometry of fate-mapped cells in the donor heart 1 week after bead injection showed that 85.12 ± 1.48% CD11b⁺ LY6C⁺ monocytes/macrophages contained fluorescent latex beads. This indicated that these *Ly6c2*⁺ monocytes/macrophages (M1, M2, and M3) within allografts are mostly recruited from the recipient (Suppl. Figure 3E). 83.32 ± 1.23% CD11b⁺ monocytes/macrophages contained fluorescent latex beads. This indicated that myeloid cells within allografts are mostly recruited from the recipient (Suppl. Figure 3E). They secreted the proinflammatory chemokine *Cxcl10* and *IL1b* (Fig. 3d). M2 and M3 both highly expressed *Lyn* (Fig. 3d), a Src family tyrosine kinase, which promoted the expression of inflammatory mediators and the production of reactive oxygen species [54, 57]. It indicated that M1, M2, and M3 played a significant role in constructing niches that drove inflammation and immune responses in AR. Based on two panels of genes associated with antigen-presenting and glycolysis (Suppl. Table 1), respectively, we computed for each monocytes/macrophages among three groups a score representing the extent to which its gene expression pattern matched that expected by the two gene panels. M1 may have a strong antigen-presenting ability (Fig. 3f), and maintained a high level of glycolysis (Fig. 3g). Both of these abilities

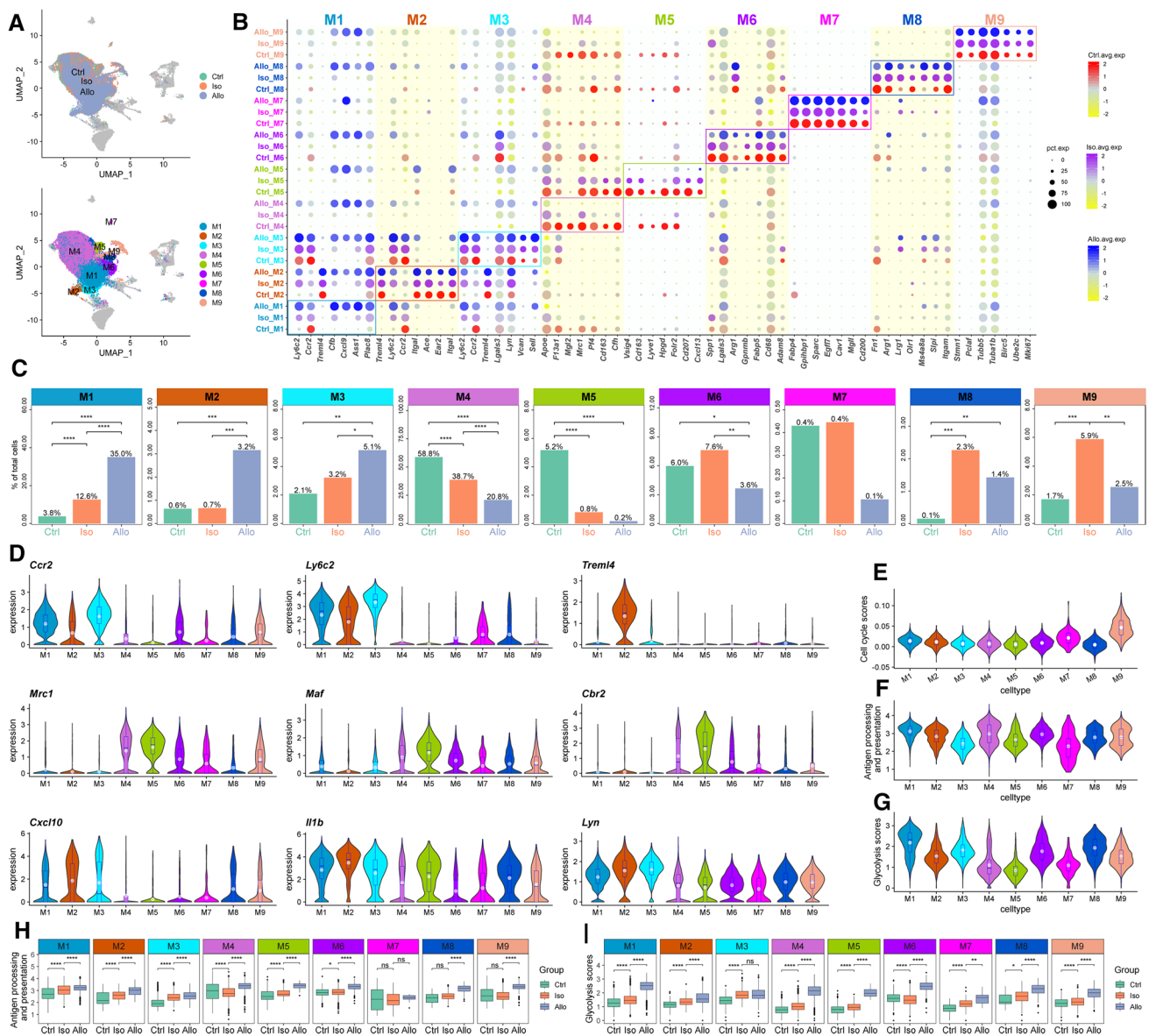


Fig. 3 Inter-group heterogeneity of monocytes/macrophages. **a** The UMAP plots of monocytes/macrophages, which were color-coded according to their group (top panel) and cell clusters (bottom panel). **b** Dot-plot heatmap showing the top expressed marker genes in each macrophage cluster. **c** The percentage change of each cluster of

monocytes/macrophages among three groups. **d** Violin plots showing the expression of representative marker genes. **e** Cell cycle scores for each macrophage cluster. **f** Antigen processing and presentation scores. **g** Glycolysis scores. **h**. Antigen processing and presentation scores in different group. **i** Glycolysis scores in different group

were particularly elevated in monocytes/macrophages of allografts (Fig. 3h, i). This was consistent with the enhanced glucose metabolism in macrophages of human hearts with AR.

M4/5/6/7 were mainly found in normal hearts, they had low expression of *Ly6c2* and *Ccr2* (Fig. 3c, d). Among them, M4 was the largest number of immune cells in normal hearts (Fig. 3c). Enrichment analysis showed M4 was associated with ERK cascade and regulation of hemopoiesis (Suppl. Figure 2A). M4 and M5 expressed genes associated with M2-like macrophages (*Mrc1*, *Maf*,

Cbr2) (Fig. 3d). These two clusters of macrophages were substantially replaced by monocyte-derived macrophages in allografts. M8 was observed mainly in the isograft, but also showed a slight increase in allografts (Fig. 3c). M8 was associated with angiogenesis and wound healing (Suppl. Figure 2A).

A latent time trajectory was built to reveal the developmental progression of monocytes/macrophages (Fig. 4a), and we found that the development of M1 was a continuum program from the control group to the Iso group to the Allo group (Fig. 4b). We identified three gene modules in M1

based on the latent time trajectory. We focused on genes that belonged to modules 1, which was mainly upregulated during the latent time on the Allo groups (Fig. 4c). Module 1 was enriched for “response to IFN- γ ”, “ATP metabolic process” and “antigen processing and presentation” (Fig. 4d). The gradually increasingly elevated genes include those associated with antigen presentation (*H2-Ab1*, *H2-Eb1*, *Psmb8*, and *Psmc2*), glycolysis (*Pkm*, *Pgk1*, *Aldoa*, and *Tpi1*), and proinflammation (*Cxcl9*, *Ccl5*, and *Il18bp*) (Fig. 4e).

We applied Single-Cell Regulatory Network Inference and Clustering (SCENIC) to assess which transcription factors (TFs) were responsible for driving the phenotypic transformation among the three groups (Fig. 4f, g). It identified macrophages in the normal hearts were mainly regulated by *Egr2* and *Mlx*. The macrophages in the Allo groups were mainly dominated by *Hmgal1*, *Sp1*, *E2f3*, *Pknx1*, and *Cebpa*.

The pro-inflammatory role of neutrophils in AR

We detected 4285 neutrophils, which were divided into 2 clusters (Fig. 5a). The proportion of N2 was similar among the three groups. The proportion of N1 was significantly increased in both Iso and Allo groups (Fig. 5b).

N1 had an elevated expression of *Srgn* (Fig. 5c). Compared with N2, N1 released high levels of proinflammatory genes *Il1b* and *Cxcl2*. Meanwhile, N1 cells highly expressed *Mmp9* (Fig. 5d). The *Mmp9* level is reported to be positively associated with the rejection of HTX [33]. N1 highly expressed genes including *Tap1*, *Tap2*, and *Tapbp*, which encode the transporter associated with the assembly and transport of MHC class I molecules (Fig. 5d). N2 had an increased expression of *Anxa5* and *Cxcl16* (Fig. 5c, d). *Anxa5* can inhibit the clearance of apoptotic cells, increase their immunogenicity [37].

To investigate the differences in regulatory relationships between neutrophils and T cells between Iso and Allo groups, we performed ligand and receptor interaction analysis. The ligand-receptor interactions with statistical differences between the two groups were visually using circular plots. The thickness of the line represents the strength of the interaction relationship (Fig. 5e). There was stronger interaction between neutrophils and T cells in allografts (Fig. 5e). N1 in allografts expressed more *Cxcl10*, interacted with *Cxcr3* on T cells. N1 in isografts had a weak and sparse antigen-presenting relationship with T cells (*H2-Q10/Cd3*), but the relationship in allografts was stronger (Fig. 5e). This suggested neutrophils had more pro-inflammatory effects in AR.

The SCENIC analysis revealed several TFs responsible for gene expression of neutrophils in allografts, including

Cebpg, *Stat5b*, *Arid3a*, *Bcl6*, and *Foxo3* (Fig. 5f). *Cebpg* and *Stat5b* were involved in neutrophil development and differentiation [18]. *Bcl6* and *Foxo3* prevented neutrophil apoptosis [48, 59], which may exacerbate inflammation in AR. *Arid3a* was reported as a potential transcription regulator of IFN- α producing in neutrophils [36].

Ccr7⁺ dendritic cells were responsible for antigen presentation

2023 DCs were detected in our study and identified as three types of DCs (Fig. 6a). The percentage of D1 decreased after HTX, the percentage of D2 increased in isografts, and D3 increased in allografts (Fig. 6b). D1 highly expressed the markers of conventional type 1 DCs (cDC1s), including *Irf8*, *Xcr1*, and *Clec9a* (Fig. 6c), and maintained a high level of lipid metabolism (Suppl. Figure 4A). D2 expressed *Cd209a* (Fig. 6c), the marker of monocyte-derived DCs, which had a role in regulating defense response and inflammatory responses (Suppl. Figure 4A). D3 was distinguished by high expression of migration-associated genes *Ccr7* and *Fscn1* (Fig. 6c), which represented as DCs moving toward draining lymph nodes. Compared to the other two clusters of DCs, D3 has stronger phagocytosis ability, especially in allografts (Fig. 6d, e).

To explore the antigen presentation role of DCs, we performed ligand and receptor analysis between dendritic cells and T cells. D1 carried *Xcr1*, connected with *Xcl1* from T cells (Fig. 6f). This interaction is an important factor in antigen cross-presentation [4]. D3 expressed *B2m* and *H2-Q4*, provided signal 1, and expressed *Cd40*, provided signal 2 for T cells activation (Fig. 6f). This indicated that D3 played a major role in antigen presentation. D3 also enhanced the interactions with T cells by expressing *Cxcl16*, *Il12b*, and *Ccl5* (Fig. 6g). SCENIC identified several TFs that may regulate gene expression of DCs in AR, including *E2f5*, *Arnt*, *Rfx1*, and *Nfatc3* (Fig. 6h). *E2f5* could regulate the cell cycle by controlling the expression of genes required for DNA synthesis and cell division [21]. *Rfx1* plays a key CIITA-independent role in protecting MHCII promoters against DNA methylation [39]. *Nfatc3* has been reported to be associated with type 1 IFN production in DCs [3].

Higher level of T cell activation was found in AR

2604T cells were clustered into three clusters (Fig. 7a). T1 increased in the Allo group compared with the other two groups (Fig. 7b). T1 cells expressed high levels of genes associated with T cell activation, including *Cd2*, *Cd28*, *Lck*, and *Coro1a*. T1 also expressed genes associated with cell division, including *Birc5*, *Stmn1*, *Mki67*, and *Top2a* (Fig. 7c). These indicated that T1 cells were constantly dividing and proliferation. T2 contained T cells

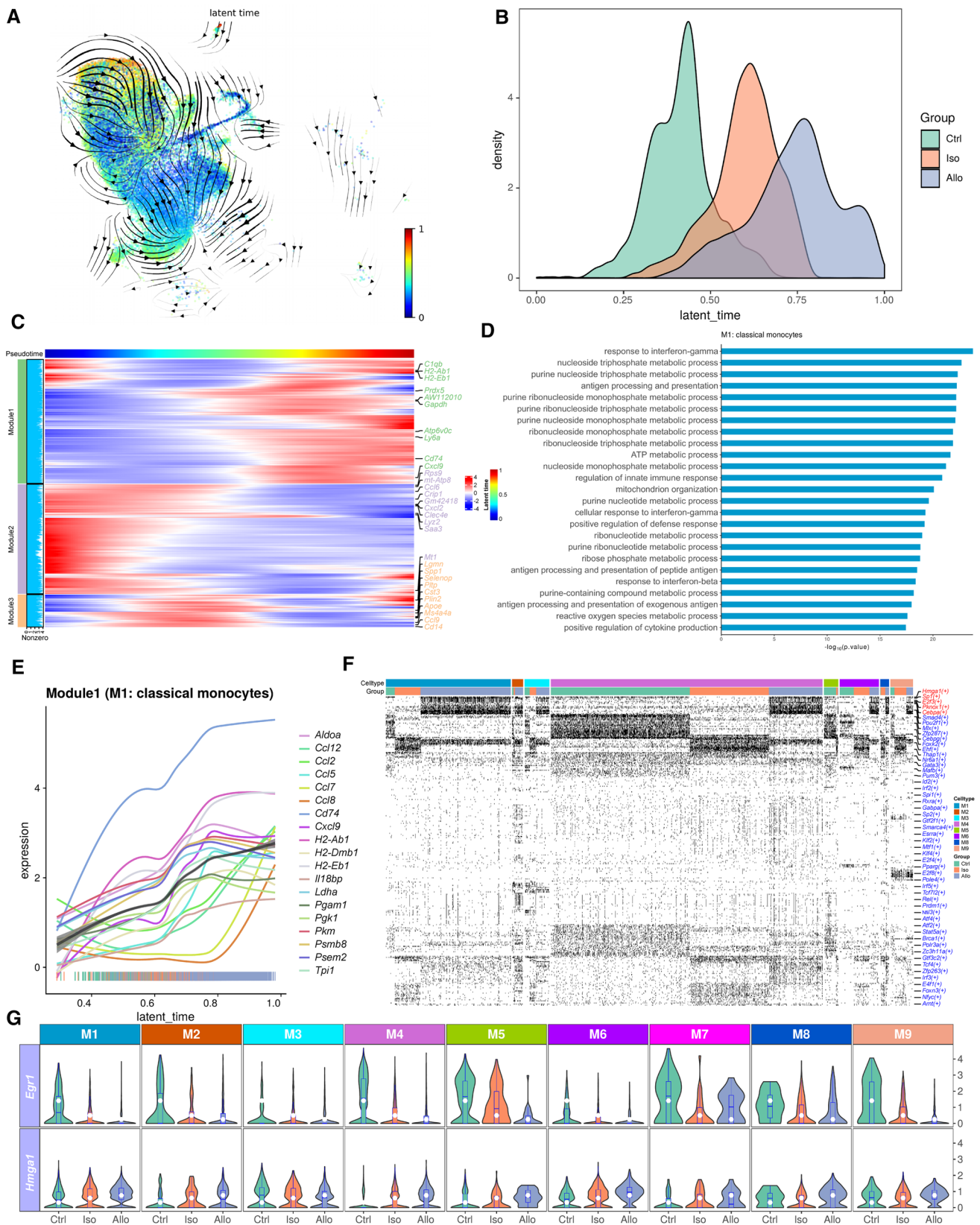


Fig. 4 RNA velocity and SCENIC analysis of monocytes/macrophages. **a** Velocity plot showing dynamic change of macrophages. **b** Density plot showing latent time of M1. **c** Heatmap for M1 over latent time. **d** Gene ontology enrichment analysis of module 1 in M1. **e** Representative genes of module 1 in M1. **f** Heatmap of the area under the curve (AUC) scores for the expression of genes regulated by TFs, as estimated using SCENIC in each macrophage cluster. **g**. Violin plots of certain TFs, *Egr1* and *Hmg1* in macrophage clusters

demonstrating higher scores of interferon-stimulated genes (ISGs), including *Ifitm3*, *Irf7*, and *Gbp2* (Fig. 7d, e). T2 cells were more abundant in normal hearts. T3 was characterized by the expression of *Trdv4*, *Tcrg-V6*, and *Il17a*, which were hallmarks of $\gamma\delta$ T cells (Fig. 7c).

T1 could be divided into two subclusters, based on the expression of *Cd4* and *Cd8a* (Fig. 7f). Gene function enrichment analysis showed that *Cd8a*⁺ T1 cells had significant cell killing ability, and *Cd4*⁺ T1 cells had a role in regulating T cell activation and cell adhesion (Fig. 7i). *Cd8a*⁺ T1 cells expressed *Xcl1* and *Ccl4* (Fig. 7g). These genes are associated with recruiting DCs [4]. *Cd8a*⁺ T1 cells expressed *Ldha* (Fig. 7g). *Ldha* was responsible for increasing the pro-inflammatory phenotype of T cells [45]. *Cd4*⁺ T1 cells had increased expression of *Hif1a* and *Got1* genes (Fig. 7g). These two genes could control the proliferation and cytotoxicity of T cells [49, 55]. Selective inhibition of *Got1* with acetic acid could ameliorate experimental autoimmune encephalomyelitis [55]. *Cd4*⁺ T1 cells highly expressed *Tnfrsf4* (Fig. 7g), which was functioned as a T cell co-stimulatory molecule [50]. Interestingly, all the above-highlighted genes had the highest expression in allografts (Fig. 7h).

SCENIC revealed that *E2f5*, *Hdac*, *Bptf*, *Tcf3*, and *Arnt* accounted for the changes of gene expression in AR (Fig. 7j). Consistent with previous reports, the HDAC inhibitor could prevent murine cardiac allograft rejection [58]. *Bptf* was also reported as an essential TF for T cell homeostasis and function [53]. *Tcf3* could promote T cells to express lower levels of inhibitory receptors and exhibit more potent cytotoxicity [13].

NK cells had higher cytotoxic effects in AR

We detected 1 cluster of 1055 NK cells. All three groups had similar proportions of NK cells, around 2% (Suppl. Figure 5A, B). NK cells expressed more granular enzyme genes in allografts, including *Gzma* and *Gzmb*, but not *Gzmc* (Suppl. Figure 5C). Among the three groups, NK cells in allografts had the highest activated levels (Suppl. Figure 5D). Gene expression network analysis based on SCENIC analysis revealed *Irf7* might play a central role in driving transcriptional activity of NK cells in allografts (Suppl. Figure 5E).

HIF1A regulated the degree of AR

Increased glycolysis levels of monocytes/macrophages were observed in allografts, but not in isografts (Fig. 3i). The expression of genes encoding glycolytic enzyme (*Pgam1*, *Gapdh*, *Aldoa*, *Eno1*, *Pgk1*), glycogen utilization (*Sorbs1*, *Gbe1*, *Pygl*), and glycolytic promoter (*Akt2*, *Stat3*, *Bnip3*) were all increased in monocytes/macrophages of allografts (Suppl. Figure 6A–C). Through SCENIC analysis, these genes were identified to be regulated by *Hif1a*, and the target score of *Hif1a* on the above genes was significantly higher in allografts than in isografts (Suppl. Figure 6D). We next explored the expression level of *Hif1a* in each cell type and each group. *Hif1a* was expressed highly in M1 and M3 (Fig. 8a). *Hif1a* was significantly up-regulated in the Allo group (Fig. 8b). Immunofluorescence staining verified that HIF1A was highly expressed in macrophages (HIF1A and CD68 positive) in allografts (Fig. 8c). These results indicated that increased cardiac macrophage glycolysis may be regulated by *Hif1a*. *Hif1a*-dependent glycolysis is critical for the induction of inflammation [8, 23], but the role of *Hif1a*-dependent glycolysis in AR has not been clarified.

To investigate the role of *Hif1a* in AR, we treated the AR mice model with the HIF1A inhibitor LW6 (Fig. 8d). The intraperitoneal injection of LW6 into AR mice for 7 days attenuated leukocyte accumulation in allografts (no treat vs. LW6 treat, 3.6 ± 0.3 vs. 2.6 ± 0.2 , $p = 0.019$, Fig. 8e, f). LW6 treatment reduced the manifestation of congestion and oedema of allografts when removed from recipients at 7 days after HTX (Suppl. Figure 7A). It also could significantly prolong the median survival time of allografts in the recipient (no treat vs. LW6 treat, 9.5 days vs. 21 days, $p < 0.001$, Suppl. Figure 7B). The expression of HIF1A was inhibited by LW6 (no treat vs. LW6 treat, 191.7 ± 55.71 mm² vs. 30.9 ± 13.5 /mm², $p = 0.001$, Fig. 8g). We induced activation of bone marrow-derived macrophages (BMDM) from C57BL/6 J mice using IFN- γ and cardiac antigens from BALB/c mice. LW6 was added into this in vitro cell culture model or not. We found inhibition of HIF1A by LW6 could significantly decrease the expression of *Pkm2*, *Gapdh*, and *Eno1* in macrophage, confirming that HIF1A can regulate the macrophage glycolytic process (Suppl. Figure 7C). We further validated whether HIF1A is expressed in human AR heart specimens. Heart samples from patients with AR were collected, compared with hearts from healthy controls. The number of HIF1A⁺ macrophages (CD68 positive) in patients with AR was increased (Fig. 8h). This suggested that HIF1A may be a target to attenuate AR.

To investigate the mechanism of high *Hif1a* expression in monocytes/macrophages under normoxia, we searched for gene that targeted *Hif1a* expression in monocytes/macrophages using scRNA-seq data. We found that *Pkm* may be the critical gene that regulates the expression of *Hif1a*

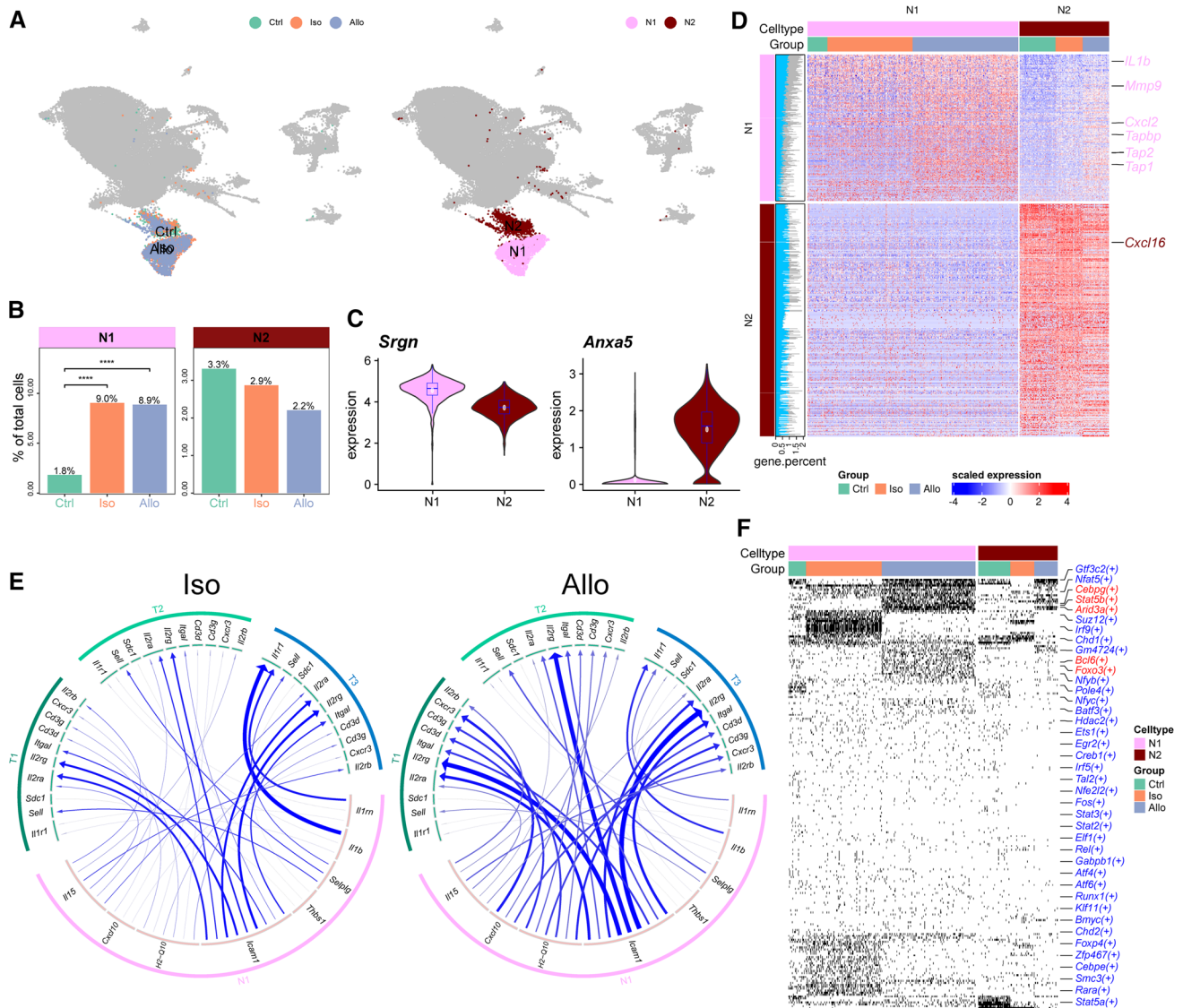


Fig. 5 Neutrophils. **a** The UMAP plots of neutrophils, which were color-coded according to their group (left panel) and cell clusters (right panel). **b** The percentage change of each cluster of neutrophils among three groups. **c** Violin plots showing the marker genes of neutrophils. **d** Gene-expression heatmap of neutrophils. **e** Ligand and

receptor interaction analysis between neutrophils and T cells among different groups. The thicker the line, the stronger the interaction. **f** Heatmap of the area under the curve (AUC) scores for the expression of genes regulated by TFs, as estimated using SCENIC in neutrophil cluster

(Suppl. Figure 7D). *Pkm* encodes pyruvate kinase, the key rate-limiting enzyme that catalyzes the conversion of phosphoenolpyruvate to pyruvate. There are two isomeric, tissue-specific forms of pyruvate kinase, PKM1 and PKM2, which are generated by alternative splicing of *Pkm* gene [56]. PKM2 rather than PKM1 is responsible for cellular metabolism of immune cells [2]. A previous study showed that PKM2 could regulate *Hif1 α* expression in LPS-induced activated macrophages [34]. This was in lined with our hypothesis that PKM2 may be the mechanism that regulates the expression of *Hif1 α* in monocytes/macrophages during AR. To verify this hypothesis, we treated the AR mice

model with PKM2 nuclear translocation blocker, TEPP46. Monocytes/macrophages (CD45⁺, CD11b⁺, and LY6C⁺) in allografts were isolated 7 days after transplantation and the expression level of *Hif1 α* in monocytes/macrophages was determined. TEPP46 could significantly reduce the expression of *Hif1 α* (Suppl. Figure 7E). These suggested that the enhancement of *Hif1 α* in monocytes/macrophages was a self-promoting process, and PKM2 played a bridging role in this process.

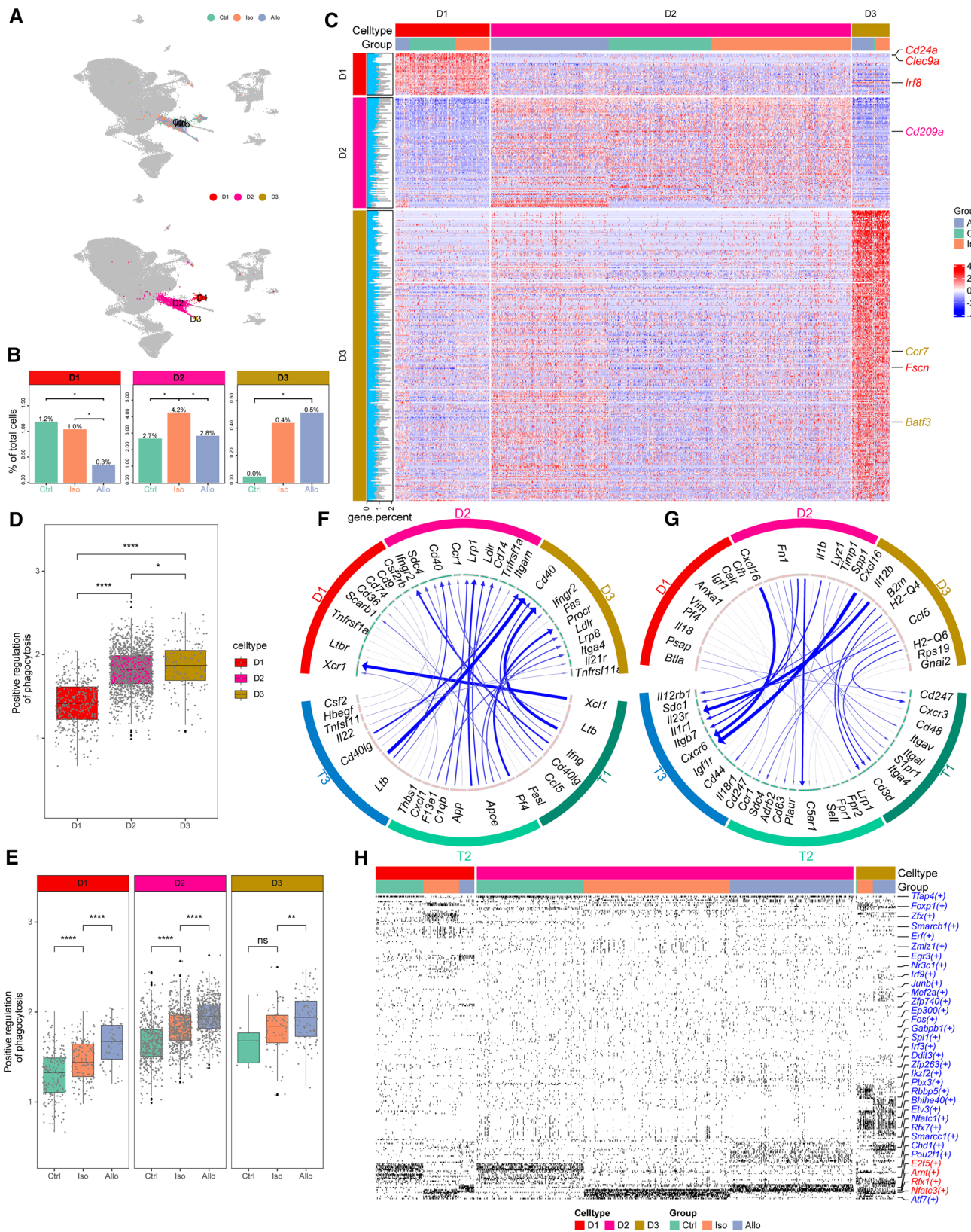


Fig. 6 Dendritic cells. **a** The UMAP plots of DCs, which were color-coded according to their group (up panel) and cell clusters (down panel). **b** The percentage change of each cluster of DCs among three groups. **c** Gene-expression heatmap of DCs. **d** Phagocytosis scores. **e**

Phagocytosis scores in different groups. **f** DCs as receptor interacted with T cells. **g** DCs as ligand interacted with T cells. **h** Heatmap of the area under the curve (AUC) scores for the expression of genes regulated by TFs, as estimated using SCENIC in DCs

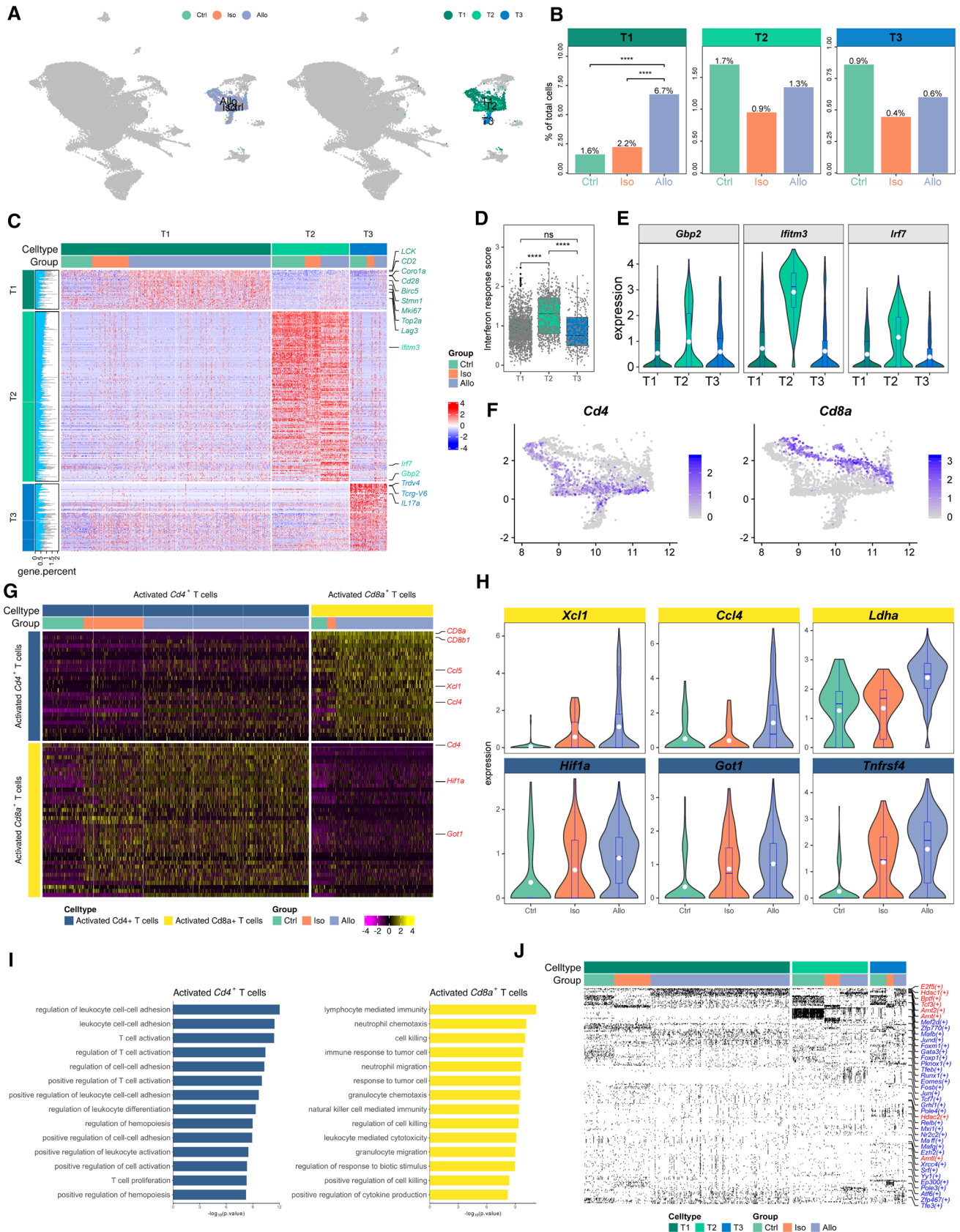


Fig. 7 T cells. **a** The UMAP plots of T cells, which were color-coded according to their group (left panel) and cell clusters (right panel). **b** The percentage change of each T cell type among three groups. **c** Gene-expression heatmap of T cells. **d** Interferon response score for each T clusters. **e** Violin plots showing the interferon response genes in each T clusters. **f** UMAP plot based on the expression of *Cd4* and *Cd8a*. **g** Gene-expression heatmap of subtype of T1 cells. **h** Violin plots showing the highly expressed genes in the *Cd4*⁺ and *Cd8a*⁺ T cells of Allo group. **i** Gene ontology enrichment analysis of *Cd4*⁺ and *Cd8a*⁺ T cells. **j** Heatmap of the area under the curve (AUC) scores for the expression of genes regulated by TFs, as estimated using SCE-NIC in T cells

Inhibition of HIF1A restricted the pro-inflammatory function of macrophages

To explore the mechanism by which HIF1A alleviated AR inflammatory infiltration, another scRNA-seq was performed on the total cardiac immune cell population (CD45⁺) in allografts from the LW6 treat group and the no treat group (Fig. 9a). After quality control, we obtained 31,852 cells, of which 16,197 cells in LW6 treat group, 15,655 cells in no treat group. 15 cell clusters were identified, including monocytes/macrophages (M, five clusters), neutrophils (one cluster), T cells (two clusters), DCs (one cluster), NK cell (one cluster), natural killer T cells (NKT, one cluster), B cells (one cluster), fibroblasts (one cluster), contaminated cells (one cluster) and mitochondrial derived cells (one cluster) (Fig. 9a). Different cell types were characterized with marker genes and specific gene expression patterns, such as *Cd3e* (T cell), *CD79a* (B cells), *Klrd1* (NK cell), *Csf1r* (M), *S100a9* (neutrophils), *H2-DMb2* (DCs), *Dcn* (fibroblast), *Birc5* (dividing cell) (Fig. 9b, Suppl. Figure 8A). Different cell types have significant different gene expression patterns (Fig. 9c). A special cluster of macrophages responding to LW6 treatment (LW6-associated macrophages) was identified. The proportion of this cluster increased after treatment (Fig. 9d). On UMAP, a different distribution existed in this cluster between the LW6 treat group and the no treat group (Fig. 9a).

The gene score analysis showed that the antigen-presenting (*B2m*, *Cd74*, *Ctsl*, *Ctss*, *H2-Aa*, *H2-Ab1*, *H2-Eb1*, *Tnf*, *Aif1*, *Cd83*) and pro-inflammatory function (*Ccl8*, *Hmox1*, *Ccl5*, *Cxcl16*, *Cxcl1*, *Thbs1*) of LW6-associated macrophages all decreased after LW6 treatment compared with no treat group (Fig. 9e). In line with scRNAseq data, LW6 could reduce the gene expression of antigen-presenting molecule (*H2-Aa*) and chemokine (*Cxcl9*) in IFN- γ and cardiac antigen induced activation of BMDM by in vitro test (Suppl. Figure 9A). This suggested that inhibition of HIF1A could attenuate the proinflammatory effect of macrophages. In support of this conclusion, the reduced infiltration of T cells in allografts treated by LW6 was confirmed (no treat vs. LW6 treat, 713.1 ± 140.7 vs. 271.2 ± 81.6 , $p < 0.001$, Fig. 9f). Therefore, inhibition of HIF1A could reduce the

antigen presenting ability and pro-inflammatory ability of macrophages, which may be the main reason for the decreased infiltration of T cells. Besides, cardiomyocytes from BALB/c mice and BMDM from C57BL/6J mice were co-cultured in vitro to verify the damage of macrophages on cardiomyocytes. LW6 treatment in this co-cultured model significantly reduced the death of cardiomyocytes (Suppl. Figure 9B). This suggested that inhibition of HIF1A can reduce the inflammatory damage of macrophages on cardiomyocytes. These results from in vivo scRNA-seq and in vitro co-culture experiments together indicated that inhibition of HIF1A could reduce immune cells recruitment and cardiomyocytes injury induced by macrophages.

Discussion

Local immune diversity in heart grafts with AR is complex, and previous studies have not revealed the full picture of the immune microenvironment. In this study, we identified several major cell types and a series of key TFs that mediate AR (Table 1). This study could provide a useful resource for finding therapeutic target of AR. Based on the elevated level of macrophage glycolysis in human hearts with AR, we particularly focused on the role of immune metabolism in AR, *Hif1 α* -dependent glycolysis was found to be served as potential targets to modulate disease progression.

Immune characteristic of AR was markedly different from the inflammation induced by IRI. Macrophages are the largest group of immune cells in the normal heart, maintain cardiac immunity and electrophysiological homeostasis [15, 22]. The subtypes of monocytes/macrophages shifted drastically after HTX, resident macrophages were predominately replaced by monocytes and monocyte-derived macrophages, we demonstrated that monocytes/macrophages in allograft were derived from recipient by fate-mapping. The proportion of M1 in AR reached 35%, which was much higher than that in isografts. Meanwhile, M2 and M3 were all increased in AR. This indicated that the infiltration of monocytes/macrophages in AR could not be explained by IRI. The pro-inflammatory effects of monocytes/macrophages in AR were mainly mediated by *Cxcl9*, *Cxcl10*, and *Il-1 β* . M1 cells upregulated the expression of antigen-presenting genes in AR, this suggested that monocytes/macrophages had a stronger ability to trigger acquired immunity in AR compared with IRI. Our results provided evidence for that monocytes/macrophages were involved in AR.

Neutrophils are usually the first leukocytes to infiltrate transplanted organs and are a well-established marker of transplant injury [38]. In our study, we found N1 in AR had a more strong connection with T cells by highly expressing

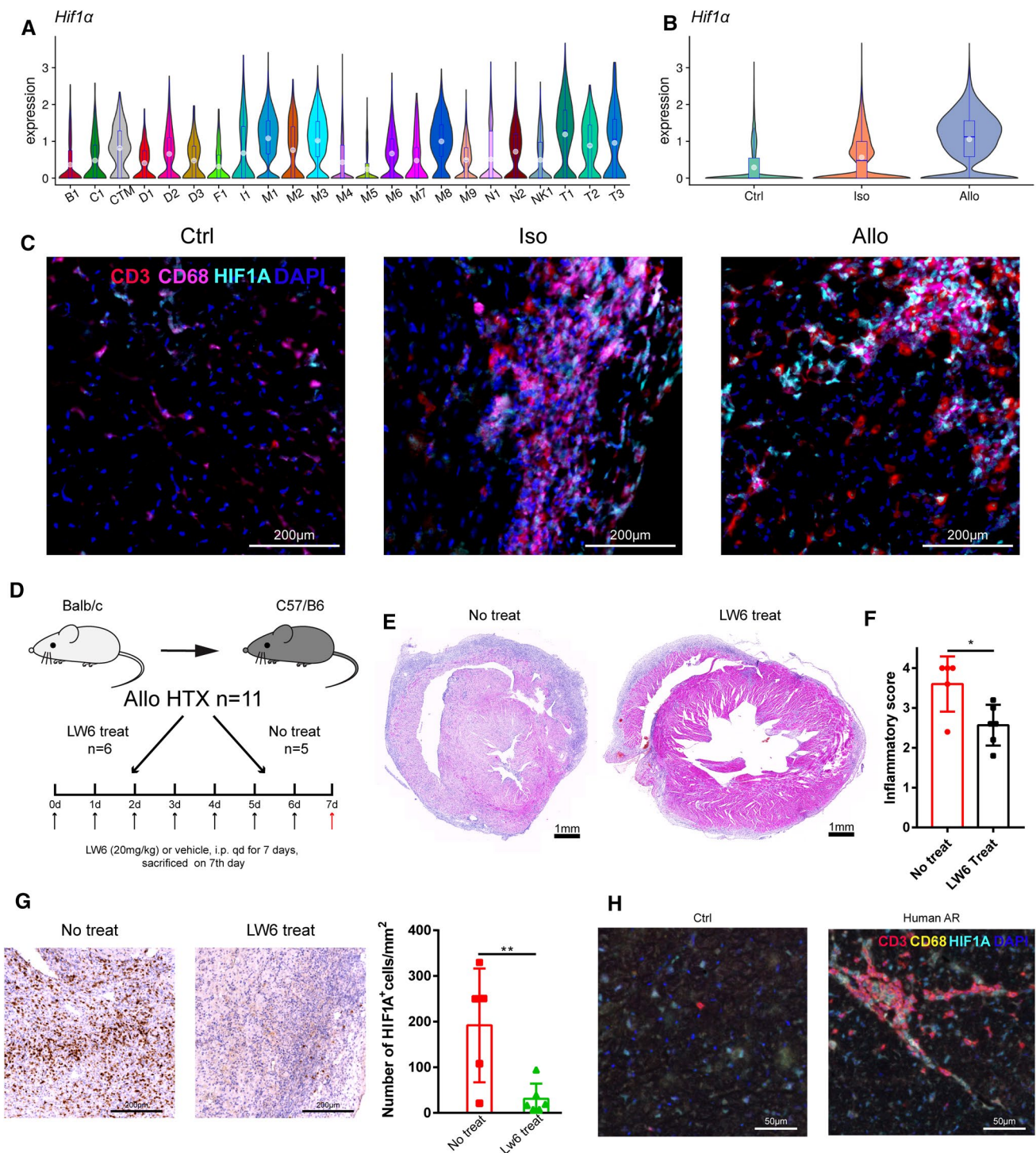


Fig. 8 The effect of HIF1A inhibitor on AR. **a** Relative average expression of *Hif1α* in each cluster. **b** Relative average expression of *Hif1α* in different groups. **c** The expression of HIF1A in T cells (CD3⁺) and macrophages (CD68⁺) in mice AR model. **d** The workflow of the LW6 treatment in the AR model. **e** The histological performances after LW6 treatment. **f** Inflammatory score after

LW6 treatment. **g** HIF1A IHC staining in allografts with and without LW6 treatment and a histogram indicating the number of HIF1A⁺ cells per mm² among the above two groups (* $p < 0.05$, ** $p < 0.01$, *** $p < 0.001$). **h** The expression of HIF1A in T cells (CD3 positive) and macrophages (CD68 positive) in human hearts of AR. *IHC* immunohistochemistry

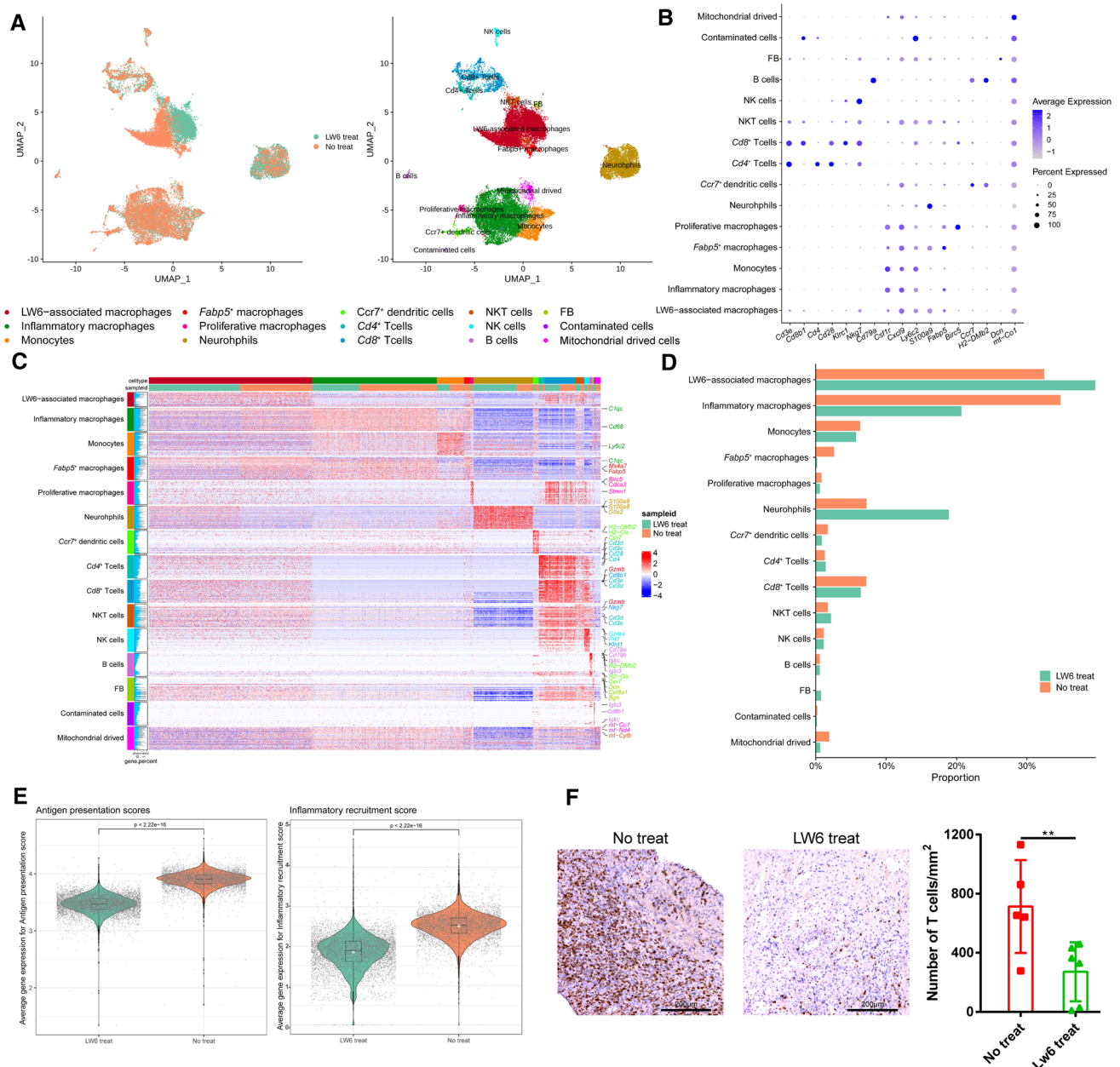


Fig. 9 scRNA-seq after LW6 treatment. **a** The UMAP plot of the 31,852 immune cells in allografts with or without LW6 treatment, which were color-coded according to their group (left panel) and cell clusters (right panel). **b** Dot-plot heatmap showing the top expressed marker genes in each cell cluster. **c** Gene-expression heatmap for 15 cell types. **d** The percentage change of each cell type between

the LW6 treat group and the no treat group. **e** Antigen presentation score and inflammatory recruitment score of LW6 associated macrophages between the two groups. **f** CD3 IHC staining in allografts with and without LW6 treatment and a histogram indicating the number of CD3+ cells per mm² among the above two groups ($p < 0.05$, $*p < 0.01$, $**p < 0.001$)

Cxcl10. This suggested that N1 in AR had a stronger inflammatory recruiting effect.

D3 cells had the strongest ability of phagocytosis in allografts, containing antigen peptide information migrated to the lymph nodes, which was guided by *Ccr7*. The anti-CCR7 monoclonal antibody was found that could prevent or treat acute graft-versus-host disease in bone marrow

transplantation model [10]. Therefore, the anti-CCR7 monoclonal antibody may also have therapeutic effects in AR, which should be further investigated.

T cells are the primary acquired immune cells that mediate the occurrence of AR [43]. Our scRNA-seq data showed that CD8+ T cells were the predominant cell type performing cell killing. The initiation of acquired immunity requires

Table 1 The summary of major cell types in AR

Cell cluster (naming)	Marker genes	Function	Peak group	Potential roles on AR	Transcription factors in AR
M1: classical monocytes	<i>Ly6c2, Ccr2, Cxcl9, Pkm, Ldha, Hif1a</i>	Antigen processing and presentation, glycolysis	Allo	Recruit T cells accumulation, antigen presentation	<i>Hmgal, Spl, E2f3, Pknox1, Cebpa</i>
M2: intermediate monocytes	<i>Ly6c2, Ccr2, Trem14, Cxcl10, Il1b</i>	Regulation of innate immune response, response to interferon	Allo	Secrete <i>Cxcl10, Lym</i> and <i>Il1b</i> , positive regulation of immune response	
M3: inflammatory monocytes	<i>Ly6c2, Ccr2, Lym, Lgals3</i>	Response to interferon, monocyte chemotaxis, inflammatory response	Allo	Secrete <i>Lym</i> , construct niches that drove inflammation and immune responses	
M4: resident macrophages	<i>ApoE, F13a1, Mrc1, Cd1163, Mgl2</i>	<i>Erk1</i> and <i>Erk2</i> cascade, regulation of hemopoiesis	Ctrl	–	
M5: <i>Vsig4</i> ⁺ macrophages	<i>Vsig4, Lyve1, Hpgd, Fcgr2</i>	Response to chemokine, regulation of inflammatory response	Ctrl	–	
M6: <i>Spp1</i> ⁺ macrophages	<i>Spp1, Lgals3</i>	Myeloid leukocyte migration	Iso and Ctrl	Regulation of myeloid leukocyte migration	
M7: <i>Fabp4</i> ⁺ macrophages	<i>Fabp4, Gp1hbp1, Sparc, Egfl7</i>	Regulation of vasculature development, regulation of angiogenesis	Iso and Ctrl	Contribute to cardiac repair for ischemia-reperfusion injury	
M8: anti-inflammatory macrophages	<i>Fnl, Arg1, Lrg1, Olr11</i>	Regulation of angiogenesis, response to wounding, wound healing	Iso and Allo	Cardiac repair	
M9: proliferative macrophages	<i>Simm1, Pclaf, Mki67</i>	Regulation of mitotic cell cycle, mitotic nuclear division	Iso	–	
N1: <i>Srgt</i> ⁺ neutrophils	<i>Srgn, Hdc, Il1b, Cxcl2, Tap1, Tap2</i>	Positive regulation of cytokine production, leukocyte migration	Iso and Allo	Play a pioneering role in the innate immune response, recruiting and activating other immune cells	<i>Cebpg, Stat5b, Arid3a, Bcl6, Foxo3</i>
N2: <i>Anxa5</i> ⁺ neutrophils	<i>Anxa5, Cxcl16</i>	Leukocyte migration, cell chemotaxis	Ctrl	Inhibit the clearance of apoptotic cells	
D1: conventional type 1 dendritic cells	<i>Irf8, Xcr1, Clec9a</i>	Antigen processing and presentation of peptide antigen via MHC class II, ribosome biogenesis	Ctrl	Antigen cross-presentation	<i>E2f5, Arnt, Rfx1, Nfatc3</i>
D2: monocyte-derived dendritic cells	<i>Cd209a</i>	Antigen processing and presentation of peptide antigen via MHC class II	Iso and Allo	Monocyte derived, antigen presentation in grafts	
D3: <i>Ccr7</i> ⁺ dendritic cells	<i>Ccr7, Fcsc1</i>	Antigen processing and presentation, T cell activation	Allo	Responsible for T cell activation, homing to the lymph nodes	

Table 1 (continued)

Cell cluster (naming)	Marker genes	Function	Peak group	Potential roles on AR	Transcription factors in AR
T1: activated T cells	<i>Cd69, Cd28, Lag3, Birc5, Mki67, Hif1a</i>	T cell activation, ribonucleoprotein complex assembly	Allo	Target and kill donor cells	<i>E2f5, Hdac, Bptf, Tcf3, Arnt</i>
T2: ISG-high T cells	<i>Ifitm3, Irf7, Gbp2</i>	T cells activation, regulation of cell adhesion	Ctrl	-	-
T3: $\gamma\delta$ T cells	<i>Trbv4, Il17a, Tcrg-v6</i>	T cell activation, lymphocyte differentiation	Allo	-	-
NK1: NK cells	<i>Gzma, Nkg7, Ncr1</i>	Natural killer cell mediated cytotoxicity, cytokine production	Allo	Release granzymes, cytotoxic effects	<i>Irf7, Nfatc3, Stat5b, Rbhp5, Tbx21</i>
B1: B cells	<i>Cd79a, Cd19</i>	B cell activation, cytoplasmic translation	Ctrl	-	-
I1: innate lymphoid cells	<i>Gata3, Il5, Il13</i>	Leukocyte differentiation, regulation of inflammatory response	Ctrl	-	-

the support of innate immunity [30]. This prompted the idea of whether it is possible to suppress the occurrence of AR by modulating innate immunity. Our data showed that monocytes/macrophages were the most abundant type of innate immune cells in allografts when occurred AR. These monocytes/macrophages were distinguished from other innate immune cells by higher levels of glycolysis. We found the glycolysis in monocytes/macrophages rely on the assist of *Hif1a*. Several studies also declared the *Hif1a*-dependent energy metabolism pathway is an adaptive behavior of immune cells under an inflammatory environment, which could promote immune cell activation, but its role in AR has not been clarified [7, 8, 40]. Isografts and allografts had the same ischemic condition, but *Hif1a* expression in isografts was not significantly elevated as that in allografts. This suggested that the elevated expression of *Hif1a* is not caused by hypoxia.

Though *Hif1a* mediates adaptive responses to hypoxia/ ischemia to protect against IRI [5], a previous study showed that cardiomyocytes had no increased expression of HIF1A in AR, this indicated that the oxygen supply was not deficient in AR [16]. Pharmacological HIF1A stabilizing preconditioning of donor hearts could activate innate immunity and increase cardiomyocyte apoptosis after 6 h after HTX [17]. All these previous studies suggested that HIF1A may be related to inflammatory cell function in AR, but the mechanism remained unknown. Similarly, mice with a myeloid cell-specific defect in *Hif1a* were unable to mount trained immunity against bacterial sepsis [7]. In our study, HIF1A inhibitors, LW6, reduced the infiltration of immune cells in allografts without using other immunosuppressive agents. LW6 treatment can reduce the antigen presenting ability and pro-inflammatory ability of macrophages, and reduce the infiltration of CD4⁺ and CD8⁺ T cells unbiasedly. This indicated that HIF1A may affect acquired immunity by regulating the innate immune response in AR. Through scRNA-seq data, we found that the expression of *Hif1a* may be regulated by *Pkm*. The expression of *Hif1a* was decreased by drug blocking PKM2 entry into the nucleus. Our study established a relationship between glycolysis and *Hif1a* in AR. HIF1A promoted the increase of glycolysis, while the key rate-limiting enzyme of glycolysis, PKM2, promoted the increase of *Hif1a* expression in macrophages under normoxic state, forming a positive feedback loop. In vitro experiments showed that inhibition of HIF1A can inhibit the pro-inflammatory effect of monocytes/macrophages, and reduced the damage of monocytes/macrophages on cardiomyocytes. Additionally, elevated glycolysis and HIF1A in macrophages was also confirmed in human heart specimens with AR, despite receiving immunosuppressive drugs. This provided a theoretical basis for attenuating AR by targeting HIF1A.

To investigate the natural reaction in AR, immunosuppressive therapy was avoided in the mouse HTX model. AR could not be developed after the use of immunosuppressive agents, despite a complete MHC mismatch [29]. HIF1A inhibitor LW6 was just used to explore the mechanism of HIF1A affecting AR, we cannot conclude that LW6 can be used in the immunosuppressive therapy of AR.

In conclusion, we described the immune microenvironment in cardiac tissues from the AR model using scRNA-seq. HIF1A could promote the occurrence of AR by regulating the activation of macrophages. We proposed HIF1A may be a promising target in the therapy of AR but need precise control. Our study also provided a set of cell atlas for further functional research in AR.

Supplementary Information The online version contains supplementary material available at <https://doi.org/10.1007/s00395-021-00904-5>.

Author contributions JPS designed and supervised the study. YC, YQH and XMH performed scRNA-seq. QC performed HTX experiments. XJL was responsible for the analysis of scRNA-seq data. XC, XXF, MHT participated in sample collection and processing. YC and XJL wrote the manuscript draft. JPS and SSH revised the manuscript. All authors read and approved the manuscript. YC, XJL, QC, and YQH contributed equally to this work.

Funding This work was supported by the National Natural Science Fund for Distinguished Young Scholars of China (82125004; to JPS) and the National Natural Science Fund for General Program of China (81670376; to JPS).

Availability of data and material The data that support the findings of this study including scRNA-seq data are available from <https://figshare.com/s/11d8b3c99165c5fd8cd3>.

Code availability R scripts for single cell data analysis are available from the corresponding author upon reasonable request.

Declarations

Conflict of interest The authors have no relevant financial or non-financial interests to disclose.

Ethics approval The use of human tissue in the present study was approved by the Human Ethics Committee of Fuwai Hospital, Chinese Academy of Medical Sciences (no. 2013-049). Written informed consent was obtained from each patient. This study was performed in accordance with the ethical standards as laid down in the 1964 Declaration of Helsinki and its later amendments or comparable ethical standards.

Consent to participate Informed consent was obtained from all individual participants included in the study.

Consent for publication Not applicable.

References

1. Aibar S, González-Blas CB, Moerman T, Huynh-Thu VA, Imrichova H, Hulselmans G, Rambow F, Marine JC, Geurts P, Aerts J, van den Oord J, Atak ZK, Wouters J, Aerts S (2017) SCENIC: single-cell regulatory network inference and clustering. *Nat Methods* 14:1083–1086. <https://doi.org/10.1038/nmeth.4463>
2. Alves-Filho JC, Pålsson-McDermott EM (2016) Pyruvate kinase M2: a potential target for regulating inflammation. *Front Immunol* 7:145. <https://doi.org/10.3389/fimmu.2016.00145>
3. Bao M, Wang Y, Liu Y, Shi P, Lu H, Sha W, Weng L, Hanabuchi S, Qin J, Plumas J, Chaperot L, Zhang Z, Liu YJ (2016) NFATC3 promotes IRF7 transcriptional activity in plasmacytoid dendritic cells. *J Exp Med* 213:2383–2398. <https://doi.org/10.1084/jem.20160438>
4. Brewitz A, Eickhoff S, Dähling S, Quast T, Bedoui S, Kroczeck RA, Kurts C, Garbi N, Barchet W, Iannacone M, Klauschen F, Kolanus W, Kaisho T, Colonna M, Germain RN, Kastentmüller W (2017) CD8(+) T cells orchestrate pDC-XCR1(+) dendritic cell spatial and functional cooperativity to optimize priming. *Immunity* 46:205–219. <https://doi.org/10.1016/j.immuni.2017.01.003>
5. Cai Z, Manalo DJ, Wei G, Rodriguez ER, Fox-Talbot K, Lu H, Zweier JL, Semenza GL (2003) Hearts from rodents exposed to intermittent hypoxia or erythropoietin are protected against ischemia–reperfusion injury. *Circulation* 108:79–85. <https://doi.org/10.1161/01.Cir.0000078635.89229.8a>
6. Chen X, Dong S, Zhang N, Chen L, Li MG, Yang PC, Song J (2017) MicroRNA-98 plays a critical role in experimental myocarditis. *Int J Cardiol* 229:75–81. <https://doi.org/10.1016/j.ijcard.2016.11.263>
7. Cheng SC, Quintin J, Cramer RA, Shepardson KM, Saeed S, Kumar V, Giamarellos-Bourboulis EJ, Martens JH, Rao NA, Aghajani-refah A, Manjeri GR, Li Y, Ifrim DC, Arts RJ, van der Veer BM, Deen PM, Logie C, O’Neill LA, Willems P, van de Veerdonk FL, van der Meer JW, Ng A, Joosten LA, Wijmenga C, Stunnenberg HG, Xavier RJ, Netea MG (2014) mTOR- and HIF-1 α -mediated aerobic glycolysis as metabolic basis for trained immunity. *Science* 345:1250684. <https://doi.org/10.1126/science.1250684>
8. Corcoran SE, O’Neill LA (2016) HIF1 α and metabolic reprogramming in inflammation. *J Clin Invest* 126:3699–3707. <https://doi.org/10.1172/jci84431>
9. Crespo-Leiro MG, Metra M, Lund LH, Milicic D, Costanzo MR, Filippatos G, Gustafsson F, Tsui S, Barge-Caballero E, De Jonge N, Frigerio M, Hamdan R, Hasin T, Hulsmann M, Nalbantgil S, Potena L, Bauersachs J, Gkouziouta A, Ruhparwar A, Ristic AD, Straburzynska-Migaj E, McDonagh T, Seferovic P, Ruschitzka F (2018) Advanced heart failure: a position statement of the Heart Failure Association of the European Society of Cardiology. *Eur J Heart Fail* 20:1505–1535. <https://doi.org/10.1002/ejhf.1236>
10. Cuesta-Mateos C, Portero-Sainz I, García-Peydró M, Alcain J, Fuentes P, Juárez-Sánchez R, Pérez-García Y, Mateu-Alberó T, Díaz-Fernández P, Vega-Piris L, Sánchez-López BA, Marcos-Jiménez A, Cardeñoso L, Gómez-García de Soria V, Toribio ML, Muñoz-Calleja C (2020) Evaluation of therapeutic targeting of CCR7 in acute graft-versus-host disease. *Bone Marrow Transplant* 55:1935–1945. <https://doi.org/10.1038/s41409-020-0830-8>
11. Dai H, Lan P, Zhao D, Abou-Daya K, Liu W, Chen W, Friday AJ, Williams AL, Sun T, Chen J, Chen W, Mortin-Toth S, Danská JS, Wiebe C, Nickerson P, Li T, Mathews LR, Turnquist HR, Nicotra ML, Gingras S, Takayama E, Kubagawa H, Shlomchik MJ, Oberbarnscheidt MH, Li XC, Lakkis FG (2020) PIRs mediate innate myeloid cell memory to nonself MHC molecules. *Science* 368:1122–1127. <https://doi.org/10.1126/science.aax4040>

12. Farbehi N, Patrick R, Dorison A, Xaymardan M, Janbandhu V, Wystub-Lis K, Ho JW, Nordon RE, Harvey RP (2019) Single-cell expression profiling reveals dynamic flux of cardiac stromal, vascular and immune cells in health and injury. *Elife*. <https://doi.org/10.7554/eLife.43882>
13. He R, Hou S, Liu C, Zhang A, Bai Q, Han M, Yang Y, Wei G, Shen T, Yang X, Xu L, Chen X, Hao Y, Wang P, Zhu C, Ou J, Liang H, Ni T, Zhang X, Zhou X, Deng K, Chen Y, Luo Y, Xu J, Qi H, Wu Y, Ye L (2016) Follicular CXCR5- expressing CD8(+) T cells curtail chronic viral infection. *Nature* 537:412–428. <https://doi.org/10.1038/nature19317>
14. Huang X, Feng Z, Jiang Y, Li J, Xiang Q, Guo S, Yang C, Fei L, Guo G, Zheng L, Wu Y, Chen Y (2019) VSIG4 mediates transcriptional inhibition of Nlrp3 and Il-1 β in macrophages. *Sci Adv* 5:eaau7426. <https://doi.org/10.1126/sciadv.aau7426>
15. Hulsmans M, Clauss S, Xiao L, Aguirre AD, King KR, Hanley A, Hucker WJ, Wülfers EM, Seemann G, Courties G, Iwamoto Y, Sun Y, Savol AJ, Sager HB, Lavine KJ, Fishbein GA, Capen DE, Da Silva N, Miquerol L, Wakimoto H, Seidman CE, Seidman JG, Sadreyev RI, Naxerova K, Mitchell RN, Brown D, Libby P, Weissleder R, Swirski FK, Kohl P, Vinegoni C, Milan DJ, Ellinor PT, Nahrendorf M (2017) Macrophages facilitate electrical conduction in the heart. *Cell* 169:510–522.e520. <https://doi.org/10.1016/j.cell.2017.03.050>
16. Keränen MA, Nykänen AI, Krebs R, Pajusola K, Tuuminen R, Alitalo K, Lemström KB (2010) Cardiomyocyte-targeted HIF-1 α gene therapy inhibits cardiomyocyte apoptosis and cardiac allograft vasculopathy in the rat. *J Heart Lung Transplant* 29:1058–1066. <https://doi.org/10.1016/j.healun.2010.05.021>
17. Keränen MA, Tuuminen R, Syrjälä S, Krebs R, Walkinshaw G, Flippin LA, Arend M, Koskinen PK, Nykänen AI, Lemström KB (2013) Differential effects of pharmacological HIF preconditioning of donors versus recipients in rat cardiac allografts. *Am J Transplant* 13:600–610. <https://doi.org/10.1111/ajt.12064>
18. Kimura A, Rieger MA, Simone JM, Chen W, Wickre MC, Zhu BM, Hoppe PS, O'Shea JJ, Schroeder T, Hennighausen L (2009) The transcription factors STAT5A/B regulate GM-CSF-mediated granulopoiesis. *Blood* 114:4721–4728. <https://doi.org/10.1182/blood-2009-04-216390>
19. Lauvau G, Chorro L, Spaulding E, Soudja SMH (2014) Inflammatory monocyte effector mechanisms. *Cell Immunol* 291:32–40. <https://doi.org/10.1016/j.cellimm.2014.07.007>
20. Li J, Diao B, Guo S, Huang X, Yang C, Feng Z, Yan W, Ning Q, Zheng L, Chen Y, Wu Y (2017) VSIG4 inhibits proinflammatory macrophage activation by reprogramming mitochondrial pyruvate metabolism. *Nat Commun* 8:1322. <https://doi.org/10.1038/s41467-017-01327-4>
21. Liban TJ, Medina EM, Tripathi S, Sengupta S, Henry RW, Buchler NE, Rubin SM (2017) Conservation and divergence of C-terminal domain structure in the retinoblastoma protein family. *Proc Natl Acad Sci USA* 114:4942–4947. <https://doi.org/10.1073/pnas.1619170114>
22. Litviňuková M, Talavera-López C, Maatz H, Reichart D, Worth CL, Lindberg EL, Kanda M, Polanski K, Heinig M, Lee M, Nadelmann ER, Roberts K, Tuck L, Fasouli ES, DeLaughter DM, McDonough B, Wakimoto H, Gorham JM, Samari S, Mahbubani KT, Saeb-Parsy K, Patone G, Boyle JJ, Zhang H, Zhang H, Viveiros A, Oudit GY, Bayraktar OA, Seidman JG, Seidman CE, Nosedá M, Hubner N, Teichmann SA (2020) Cells of the adult human heart. *Nature* 588:466–472. <https://doi.org/10.1038/s41586-020-2797-4>
23. Liu L, Lu Y, Martinez J, Bi Y, Lian G, Wang T, Milasta S, Wang J, Yang M, Liu G, Green DR, Wang R (2016) Proinflammatory signal suppresses proliferation and shifts macrophage metabolism from Myc-dependent to HIF1 α -dependent. *Proc Natl Acad Sci USA* 113:1564–1569. <https://doi.org/10.1073/pnas.1518000113>
24. Lund LH, Edwards LB, Kucheryavaya AY, Benden C, Christie JD, Dipchand AI, Dobbels F, Goldfarb SB, Levvey BJ, Meiser B, Yusef RD, Stehlik J (2014) The registry of the International Society for Heart and Lung Transplantation: thirty-first official adult heart transplant report—2014; focus theme: retransplantation. *J Heart Lung Transplant* 33:996–1008. <https://doi.org/10.1016/j.healun.2014.08.003>
25. Maenosono R, Nian Y, Iske J, Liu Y, Minami K, Rommel T, Martin F, Abdi R, Azuma H, Rosner BA, Zhou H, Milford E, Elkhali A, Tullius SG (2021) Recipient sex and estradiol levels affect transplant outcomes in an age-specific fashion. *Am J Transplant* 21:3239–3255. <https://doi.org/10.1111/ajt.16611>
26. Malone AF, Humphreys BD (2019) Single-cell transcriptomics and solid organ transplantation. *Transplantation* 103:1776–1782. <https://doi.org/10.1097/TP.0000000000002725>
27. McKay D, Shigeoka A, Rubinstein M, Surh C, Sprent J (2006) Simultaneous deletion of MyD88 and Trif delays major histocompatibility and minor antigen mismatch allograft rejection. *Eur J Immunol* 36:1994–2002. <https://doi.org/10.1002/eji.200636249>
28. McNerney ME, Lee KM, Zhou P, Molinero L, Mashayekhi M, Guziar D, Sattar H, Kuppireddi S, Wang CR, Kumar V, Alegre ML (2006) Role of natural killer cell subsets in cardiac allograft rejection. *Am J Transplant* 6:505–513. <https://doi.org/10.1111/j.1600-6143.2005.01226.x>
29. Moffatt SD, Metcalfe SM (2000) Comparison between tacrolimus and cyclosporine as immunosuppressive agents compatible with tolerance induction by CD4/CD8 blockade. *Transplantation* 69:1724–1726. <https://doi.org/10.1097/00007890-200004270-00033>
30. Murphy SP, Porrett PM, Turka LA (2011) Innate immunity in transplant tolerance and rejection. *Immunol Rev* 241:39–48. <https://doi.org/10.1111/j.1600-065X.2011.01009.x>
31. O'Neill LA, Kishton RJ, Rathmell J (2016) A guide to immunometabolism for immunologists. *Nat Rev Immunol* 16:553–565. <https://doi.org/10.1038/nri.2016.70>
32. Ochando J, Ordikhani F, Boros P, Jordan S (2019) The innate immune response to allotransplants: mechanisms and therapeutic potentials. *Cell Mol Immunol* 16:350–356. <https://doi.org/10.1038/s41423-019-0216-2>
33. Ogawa M, Suzuki J, Hishikari K, Takayama K, Tanaka H, Isobe M (2008) Clarithromycin attenuates acute and chronic rejection via matrix metalloproteinase suppression in murine cardiac transplantation. *J Am Coll Cardiol* 51:1977–1985. <https://doi.org/10.1016/j.jacc.2008.01.050>
34. Palsson-McDermott EM, Curtis AM, Goel G, Lauterbach MA, Sheedy FJ, Gleeson LE, van den Bosch MW, Quinn SR, Domingo-Fernandez R, Johnston DG, Jiang JK, Israelsen WJ, Keane J, Thomas C, Clish C, Vander Heiden M, Xavier RJ, O'Neill LA (2015) Pyruvate kinase M2 regulates Hif-1 α activity and IL-1 β induction and is a critical determinant of the warburg effect in LPS-activated macrophages. *Cell Metab* 21:65–80. <https://doi.org/10.1016/j.cmet.2014.12.005>
35. Raichlin E, Edwards BS, Kremers WK, Clavell AL, Rodeheffer RJ, Frantz RP, Pereira NL, Daly RC, McGregor CG, Lerman A, Kushwaha SS (2009) Acute cellular rejection and the subsequent development of allograft vasculopathy after cardiac transplantation. *J Heart Lung Transplant* 28:320–327. <https://doi.org/10.1016/j.healun.2009.01.006>
36. Ratliff ML, Garton J, Garman L, Barron MD, Georgescu C, White KA, Chakravarty E, Wren JD, Montgomery CG, James JA, Webb CF (2019) ARID3a gene profiles are strongly associated with human interferon alpha production. *J Autoimmun* 96:158–167. <https://doi.org/10.1016/j.jaut.2018.09.013>

37. Rosenbaum S, Kreft S, Etich J, Frie C, Stermann J, Grskovic I, Frey B, Mielenz D, Pöschl E, Gaipf U, Paulsson M, Brachvogel B (2011) Identification of novel binding partners (annexins) for the cell death signal phosphatidylserine and definition of their recognition motif. *J Biol Chem* 286:5708–5716. <https://doi.org/10.1074/jbc.M110.193086>
38. Scozzi D, Ibrahim M, Menna C, Krupnick AS, Kreisel D, Gelman AE (2017) The role of neutrophils in transplanted organs. *Am J Transplant* 17:328–335. <https://doi.org/10.1111/ajt.13940>
39. Seguí-Estévez Q, De Palma R, Krawczyk M, Leimgruber E, Villard J, Picard C, Tagliamacco A, Abbate G, Gorski J, Nocera A, Reith W (2009) The transcription factor RFX protects MHC class II genes against epigenetic silencing by DNA methylation. *J Immunol* 183:2545–2553. <https://doi.org/10.4049/jimmunol.0900376>
40. Shi LZ, Wang R, Huang G, Vogel P, Neale G, Green DR, Chi H (2011) HIF1 α -dependent glycolytic pathway orchestrates a metabolic checkpoint for the differentiation of TH17 and Treg cells. *J Exp Med* 208:1367–1376. <https://doi.org/10.1084/jem.20110278>
41. Shirakawa K, Endo J, Kataoka M, Katsumata Y, Yoshida N, Yamamoto T, Isobe S, Moriyama H, Goto S, Kitakata H, Hiraide T, Fukuda K, Sano M (2018) IL (interleukin)-10-STAT3-galectin-3 axis is essential for osteopontin-producing reparative macrophage polarization after myocardial infarction. *Circulation* 138:2021–2035. <https://doi.org/10.1161/circulationaha.118.035047>
42. Silvis MJM, Kaffka Genaam D, Dengler SE, Odille CA, Mishra M, van der Kaaij NP, Doevendans PA, Sluijter JPG, de Kleijn DPV, de Jager SCA, Bosch L, van Hout GPJ (2020) Damage-associated molecular patterns in myocardial infarction and heart transplantation: the road to translational success. *Front Immunol* 11:599511. <https://doi.org/10.3389/fimmu.2020.599511>
43. Siu JHY, Surendrakumar V, Richards JA, Pettigrew GJ (2018) T cell allorecognition pathways in solid organ transplantation. *Front Immunol* 9:2548. <https://doi.org/10.3389/fimmu.2018.02548>
44. Soderlund C, Ohman J, Nilsson J, Higgins T, Kornhall B, Johansson L, Radegran G (2014) Acute cellular rejection the first year after heart transplantation and its impact on survival: a single-centre retrospective study at Skane University Hospital in Lund 1988–2010. *Transpl Int* 27:482–492. <https://doi.org/10.1111/tri.12284>
45. Souto-Carneiro MM, Klika KD, Abreu MT, Meyer AP, Saffrich R, Sandhoff R, Jennemann R, Kraus FV, Tykocinski LO, Eckstein V, Carvalho L, Kriegsmann M, Giese T, Lorenz HM, Carvalho RA (2020) Proinflammatory profile of autoimmune CD8(+) T cells relies on increased LDHA activity and aerobic glycolysis. *Arthritis Rheumatol*. <https://doi.org/10.1002/art.41420>
46. Stehlik J, Kobashigawa J, Hunt SA, Reichenspurner H, Kirklin JK (2018) Honoring 50 years of clinical heart transplantation in circulation: in-depth state-of-the-art review. *Circulation* 137:71–87. <https://doi.org/10.1161/circulationaha.117.029753>
47. Stuart T, Butler A, Hoffman P, Hafemeister C, Papalexi E, Mauck WM 3rd, Hao Y, Stoeckius M, Smibert P, Satija R (2019) Comprehensive integration of single-cell data. *Cell* 177:1888–1902. <https://doi.org/10.1016/j.cell.2019.05.031>
48. Turrel-Davin F, Tournadre A, Pachot A, Arnaud B, Cazalis MA, Mougou B, Miossec P (2010) FoxO3a involved in neutrophil and T cell survival is overexpressed in rheumatoid blood and synovial tissue. *Ann Rheum Dis* 69:755–760. <https://doi.org/10.1136/ard.2009.109991>
49. Tyrakis PA, Palazon A, Macias D, Lee KL, Phan AT, Veliça P, You J, Chia GS, Sim J, Doedens A, Abelanet A, Evans CE, Griffiths JR, Poellinger L, Goldrath AW, Johnson RS (2016) S-2-hydroxyglutarate regulates CD8(+) T-lymphocyte fate. *Nature* 540:236–241. <https://doi.org/10.1038/nature20165>
50. Webb GJ, Hirschfield GM, Lane PJ (2016) OX40, OX40L and autoimmunity: a comprehensive review. *Clin Rev Allergy Immunol* 50:312–332. <https://doi.org/10.1007/s12016-015-8498-3>
51. Weber BN, Kobashigawa JA, Givertz MM (2017) Evolving areas in heart transplantation. *JACC Heart Fail* 5:869–878. <https://doi.org/10.1016/j.jchf.2017.10.009>
52. Wolock SL, Lopez R, Klein AM (2019) Scrublet: computational identification of cell doublets in single-cell transcriptomic data. *Cell Syst* 8:281–291.e289. <https://doi.org/10.1016/j.cels.2018.11.005>
53. Wu B, Wang Y, Wang C, Wang GG, Wu J, Wan YY (2016) BPTF is essential for T cell homeostasis and function. *J Immunol* 197:4325–4333. <https://doi.org/10.4049/jimmunol.1600642>
54. Xu C, Zhang C, Ji J, Wang C, Yang J, Geng B, Zhao T, Zhou H, Mu X, Pan J, Hu S, Lv Y, Chen X, Wen H, You Q (2018) CD36 deficiency attenuates immune-mediated hepatitis in mice by modulating the proapoptotic ef. *Hepatology* (Baltimore, MD) 67:1943–1955. <https://doi.org/10.1002/hep.29716>
55. Xu T, Stewart KM, Wang X, Liu K, Xie M, Ryu JK, Li K, Ma T, Wang H, Ni L, Zhu S, Cao N, Zhu D, Zhang Y, Akassoglou K, Dong C, Driggers EM, Ding S (2017) Metabolic control of T(H)17 and induced T(reg) cell balance by an epigenetic mechanism. *Nature* 548:228–233. <https://doi.org/10.1038/nature23475>
56. Zahra K, Dey T, Ashish MSP, Pandey U (2020) Pyruvate kinase M2 and cancer: the role of PKM2 in promoting tumorigenesis. *Front Oncol* 10:159. <https://doi.org/10.3389/fonc.2020.00159>
57. Zewinger S, Reiser J, Jankowski V, Alansary D, Hahm E, Triem S, Klug M, Schunk SJ, Schmit D, Kramann R, Körbel C, Ampfo E, Laschke MW, Selejan S-R, Paschen A, Herter T, Schuster S, Silbernagel G, Sester M, Sester U, Aßmann G, Bals R, Kostner G, Jähnen-Dechent W, Menger MD, Rohrer L, März W, Böhm M, Jankowski J, Kopf M, Latz E, Niemyer BA, Fliser D, Laufs U, Speer T (2020) Apolipoprotein C3 induces inflammation and organ damage by alternative inflammasome activation. *Nat Immunol* 21:30–41. <https://doi.org/10.1038/s41590-019-0548-1>
58. Zhang X, Han S, Kang Y, Guo M, Hong S, Liu F, Fu S, Wang L, Wang QX (2012) SAHA, an HDAC inhibitor, synergizes with tacrolimus to prevent murine cardiac allograft rejection. *Cell Mol Immunol* 9:390–398. <https://doi.org/10.1038/cmi.2012.28>
59. Zhu B, Zhang R, Li C, Jiang L, Xiang M, Ye Z, Kita H, Melnick AM, Dent AL, Sun J (2019) BCL6 modulates tissue neutrophil survival and exacerbates pulmonary inflammation following influenza virus infection. *Proc Natl Acad Sci U S A* 116:11888–11893. <https://doi.org/10.1073/pnas.1902310116>
60. Zou Y, Steurer W, Klima G, Obrist P, Margreiter R, Brandacher G (2002) Estradiol enhances murine cardiac allograft rejection under cyclosporin and can be antagonized by the antiestrogen tamoxifen. *Transplantation* 74:354–357. <https://doi.org/10.1097/00007890-200208150-00010>